European Journal of Medicinal Chemistry 155 (2018) 736–753

Contents lists available at ScienceDirect

European Journal of Medicinal Chemistry

journal homepage: http://www.elsevier.com/locate/ejmech

Research paper

Synthesis and biological evaluations of marine oxohexadecenoic acids: PPARα/γ dual agonism and anti-diabetic target gene effects

Thomas Sæther [a, *], Steinar M. Paulsen [b], Jørn E. Tungen [c], Anders Vik [c], Marius Aursnes [c], Torgeir Holen [a], Trond Vidar Hansen [c], Hilde I. Nebb [a]

[a] Department of Nutrition, Institute of Basic Medical Sciences, University of Oslo, N-0317 Oslo, Norway
[b] MabCent-SFI, UiT The Arctic University of Norway, N-9037 Tromsø, Norway
[c] School of Pharmacy, Department of Pharmaceutical Chemistry, University of Oslo, N-0316 Oslo, Norway

ARTICLE INFO

Article history:
Received 4 May 2018
Received in revised form
7 June 2018
Accepted 13 June 2018
Available online 18 June 2018

ABSTRACT

Obesity and associated disorders such as metabolic syndrome and type 2 diabetes (T2D) have reached epidemic proportions. Several natural products have been reported as Peroxisome Proliferator-Activated Receptor (PPAR) agonists, functioning as lead compounds towards developing new anti-diabetic drugs due to adverse side effects of existing PPAR drugs. We recently isolated and identified (7*E*)-9-oxohexadec-7-enoic acid (**1**) and (10*E*)-9-oxohexadec-10-enoic acid (**2**) from the marine algae *Chaetoceros karianus*. Herein we report the total synthesis, pharmacological characterization, and biological evaluations of these naturally occurring oxo-fatty acids (oFAs). The syntheses of **1** and **2** afforded sufficient material for extensive biological evaluations. Both oFAs show an appreciable dose-dependent activation of PPARα and -γ, with EC_{50} values in the micromolar range, and an ability to regulate important PPAR target genes in hepatocytes and adipocytes. Moreover, both **1** and **2** are able to drive adipogenesis when evaluated in the Simpson-Golabi-Behmel syndrome (SGBS) pre-adipocyte cell model, but with lowered expression of adipocyte markers and reduced lipid accumulation compared to the drug rosiglitazone. This seems to be caused by a transient upregulation of PPARγ and C/EBPα expression. Importantly, whole transcriptome analysis shows that both compounds induce anti-diabetic gene programs in adipocytes by upregulating insulin-sensitizing adipokines and repressing pro-inflammatory cytokines.

1. Introduction

Obesity and associated disorders, such as metabolic syndrome and type 2 diabetes (T2D), constitute a serious health problem. The WHO estimates that there are more than 2 billion overweight adults worldwide, half of whom are clinically obese [1]. Over 300 million people suffer from T2D, a number that will continue to grow due to changes in dietary patterns and a more sedentary lifestyle. Understanding the mechanisms of metabolic control in order to prevent and treat these disorders is therefore a top research priority. Present anti-diabetic medications include several drug classes, such as metformin, DPP-4 inhibitors, GLP-1 analogs/agonists, SGLT-2 inhibitors, as well as drugs targeting the peroxisome proliferator-activated receptors (PPARs).

PPARs are nuclear receptors that heterodimerize with the retinoid X receptor (RXR) and regulate target gene expression in response to lipids such as unsaturated fatty acids, phospholipids, eicosanoids, and oxygenated fatty acids [2]. Upon ligand activation, the PPARs undergo conformational changes that facilitate the dissociation of transcriptional co-repressors like SMRT and NCoR [3,4], and recruitment of transcriptional co-activators and co-activator complexes, which include factors such as p300/CBP, SRC-1, and PGC-1α [4,5]. Additionally, posttranslational modifications alter the structural conformation of the receptors thereby modifying the affinity for co-regulators that determine whether a target gene is induced or repressed. In humans the PPAR isoforms PPARα (NR1C1) and -γ (NR1C3) are mainly expressed in liver and adipose tissue, respectively, while PPARδ (NR1C2) is more ubiquitously expressed [6,7]. When PPARγ is ligand-activated it induces adipocyte growth and differentiation by transcriptionally regulating target genes involved in lipogenesis and lipid storage [8–10].

* Corresponding author.
E-mail address: thomas.sather@medisin.uio.no (T. Sæther).

https://doi.org/10.1016/j.ejmech.2018.06.034

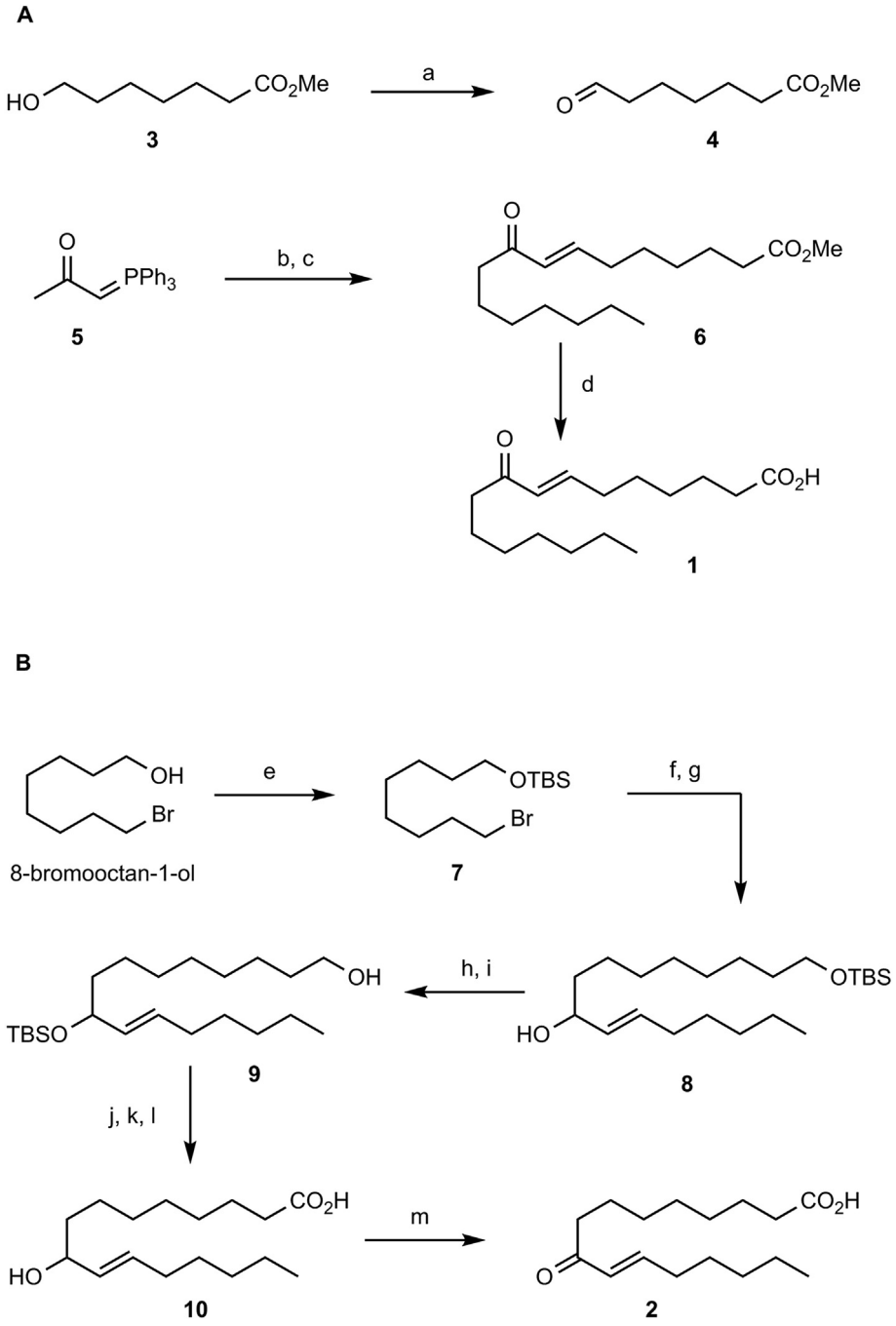

Scheme 1. Reagents and conditions: (a) $(COCl)_2$, DMSO, Et_3N, CH_2Cl_2, 81%; (b) *n*-BuLi, THF, −78 °C, 1−bromohexane; (c) **4**, THF, 53% (two steps); (d) Lipase from *Pseudomonas cepacia*, pH = 7.2, 64%; (e) TBSCl, imidazole, MeCN, 90%; (f) Mg, I_2 cat., THF; (g) (*E*)-2-octenal, THF, 70% (two steps); (h) TBSCl, imidazole, DMF, 91%; (i) TFA, H_2O, THF, 65%; (j) Dess-Martin periodinane, $NaHCO_3$, CH_2Cl_2; (k) $NaClO_2$, NaH_2PO_4, MeCN, 2-methyl-2-butene, H_2O; (l) TBAF, THF, 67% (three steps); (m) MnO_2, Celite, CH_2Cl_2, 15%.

Moreover, activation of PPARγ maintains normal insulin sensitivity through upregulation and secretion of adipokines such as adiponectin and leptin from adipose tissue [11]. In parallel, PPARα increases lipid uptake and energy expenditure in liver by upregulating gene targets involved in fatty acid transport, activation and oxidation [12,13]. We recently identified the two isomeric oxo-fatty acids (7*E*)-9-oxohexadec-7-enoic acid (**1**) and (10*E*)-9-oxohexadec-10-enoic acid (**2**) from the marine algae *Chaetoceros karianus*, and demonstrated that they display dual PPAR α/γ agonist activity [14]. Several synthetic PPAR drugs are already in clinical use, like the lipid-lowering fibrates, acting as PPARα activators, and the anti-diabetic thiazolidinediones (TZDs), targeting PPARγ. However, some of the isoform-specific PPAR agonists like clofibrate, rosiglitazone and pioglitazone have demonstrated adverse effects such as hepatotoxicity [15,16], pulmonary edema [17], myocardial infarction [18], weight gain [19], reduced bone density [20], and bladder and prostate cancer [21,22]. A suggested way out has been to identify natural products as candidate compounds with potency for both PPARα and -γ, aiming at maximizing the beneficial effects, while minimizing the adverse. Several promising dual agonists

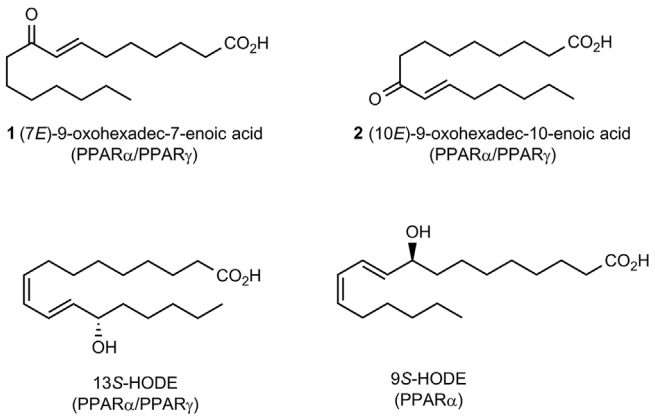

Fig. 1. Structure of (7*E*)-9-oxohexadec-7-enoic acid (**1**) and (10*E*)-9-oxohexadec-10-enoic acid (**2**), (9*Z*,11*E*,13*S*)-13-Hydroxyoctadeca-9,11-dienoic acid (13*S*-HODE), and (9*S*,10*E*,12*Z*)-9-Hydroxyoctadeca-10,12-dienoic acid (9*S*-HODE).

display significant improvement in both glycemic as well as dyslipidemic parameters with no evidence of conventional side effects [23–27]. In this aspect, natural products are of interest. Some natural occurring fatty acid PPAR-agonists are depicted below.

In this paper we report the synthesis, pharmacological characterization, and extensive biological evaluations of the oxo-fatty acids **1** and **2**.

2. Results and discussion

2.1. Chemistry

The synthesis towards (7*E*)-9-oxohexadec-7-enoic acid (**1**) started with known methyl 7-hydroxyheptanoate (**3**) [28,29] (Scheme 1). Swern oxidation of **3** afforded **4** in 81% yield. Next the commercially available phosphorane **5** was treated with *n*-BuLi and 1-bromohexane to afford the hexyl substituted intermediate of **5** that was reacted with aldehyde **4** in an *E*-selective Wittig-reaction. This gave methyl (*E*)-9-oxohexadec-7-enoate (**6**) in 53% yield from **3**. The hydrolysis of **6** to **1** proved more challenging than anticipated as several conditions failed to produce the natural product **1** due to the formation of polymeric material. However, the acid **1** was formed when **6** was added to a phosphate buffer solution (pH = 7.2, 37 °C) containing lipase from *Pseudomonas cepacia*. The spectral data confirmed the structure of **1** with the *E*-configuration ($J = 15.9$ Hz).

The synthetic approach for making **1** was not amendable for making (10*E*)-9-oxohexadec-10-enoic acid (**2**). The α,β-unsaturated ketone moiety in **2** was proven to be quite labile. Hence, an alternative synthetic route was developed. First, known **7** [30] was

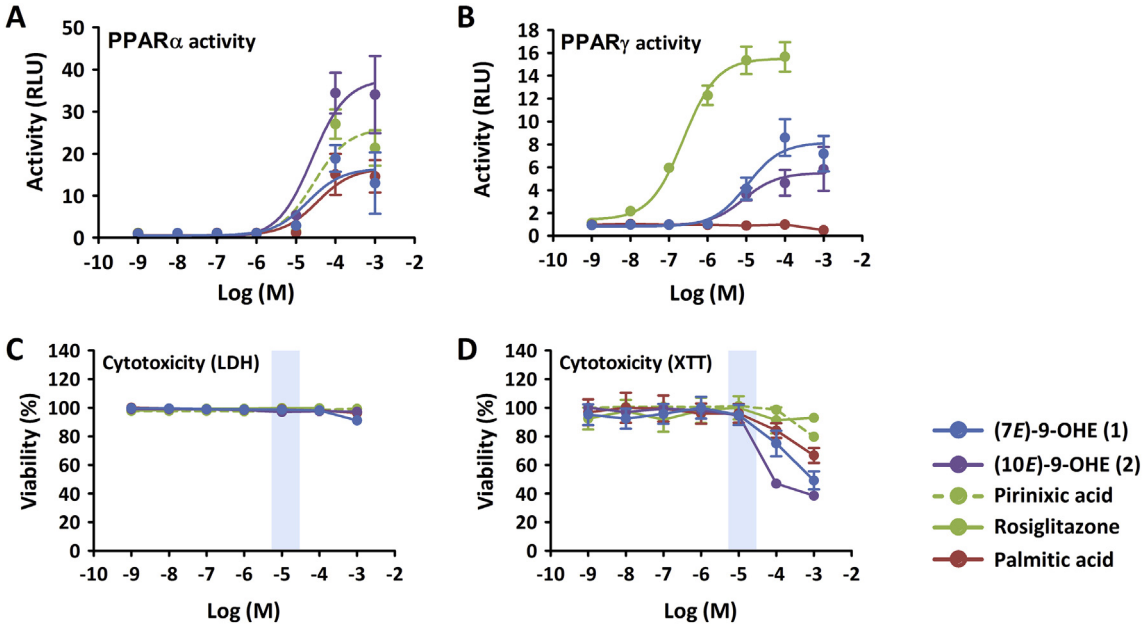

Fig. 2. The synthetic oxo-fatty acids (7*E*)-9-oxohexadec-7-enoic acid (1) and (10*E*)-9-oxohexadec-10-enoic acid (2) activate PPARα and -γ and show low cytotoxicity. Dose-response of **1** (7*E*)-9-OHE and **2** (10*E*)-9-OHE, compared to pirinixic acid, rosiglitazone and palmitic acid on **(A)** PPARα activity and **(B)** PPARγ activity. The assays were run with Gal4-DBD-NR-LBD chimeric constructs in COS-1 cells, using LBD from human PPARα and PPARγ, respectively. **(C)** Corresponding cytotoxicity data were obtained by measuring lactate dehydrogenase (LDH) in media or **(D)** by running XTT assays. The results are shown as mean ± SEM. The data represent three biological replicates run in quadruplicates. RLU: relative light units.

Table 1
PPAR EC_{50} values and corresponding cytotoxicity of the oxo-fatty acids.

Compound	PPARα agonism EC_{50} (μM)	PPARγ agonism EC_{50} (μM)	Viability at EC_{50} LDH (%)	Viability at EC_{50} XTT (%)
1	20	10	>95	>90
2	26	8.5	>95	>90
Pirinixic acid	39	n.d.	>95	>95
Rosiglitazone	n.d.	0.2	>95	>95
Palmitic acid	35	n.d.	>95	>90

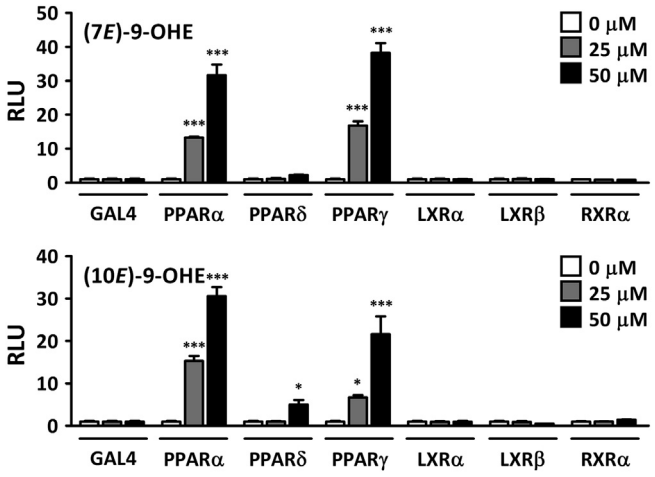

Fig. 3. The oxo-fatty acids 1 and 2 display PPARα/γ dual specificity. The assays were run with Gal4-DBD-NR-LBD chimeric constructs in COS-1 cells, using the ligand binding domain (LBD) from human nuclear receptors. The doses used were 0, 25 and 50 μM of **1** (7*E*)-9-OHE and **2** (10*E*)-9-OHE, respectively. The results are shown as mean ± SEM. The data represent three biological replicates run in quadruplicates. RLU: relative light units. $^{*}p < 0.05$, $^{**}p < 0.05$, $^{***}p < 0.001$.

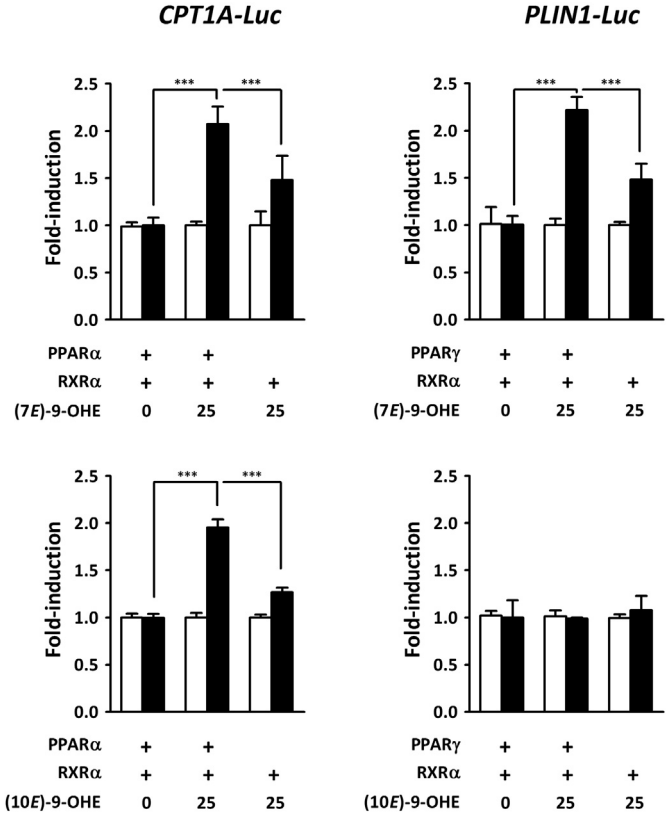

Fig. 4. The oxo-fatty acids 1 and 2 activate human natural promoters in a PPAR/PPRE-depend manner. COS-1 cells were transfected with full-length PPARα, the heterodimerization partner RXRα and a *CPT1A*-driven reporter, with or without a functional PPAR recognition element (PPRE) or PPARγ, RXRα and a *PLIN1*-driven reporter, with (black bars) or without (white bars) a functional PPRE. The cells were then treated with **1** (7*E*)-9-OHE or **2** (10*E*)-9-OHE for 18 h. The results are shown as mean ± SEM. The data represent three biological replicates run in quadruplicates. RLU: relative light units. $^{***}p < 0.001$.

transferred into its Grignard reagent that was added to a THF-solution of commercially available (*E*)-2-octenal. This gave the allylic alcohol **8**. Hence, alcohol **8** was converted into the bis-TBS ether using standard conditions (TBSCl, imidazole) that was mono-deprotected using aqueous TFA. This gave **9** that was oxidized to the aldehyde using the Dess-Martin reaction. A Lindgren-Pinnick oxidation of the formed aldehyde followed by deprotection of the TBS-group afforded **10**. Oxidation of the allylic alcohol was best achieved using electrolytically activated MnO_2 that gave the natural product **2**, albeit in 15% yield. The spectral data confirmed the structure of **2**. All efforts to improve the yield of **2** were fruitless. The total yield of **2** was 4% over nine steps from 8-bromooctan-1-ol.

2.2. Dose-response and toxicity

We started by evaluating oxo-fatty acid (oFA) **1** and **2** with respect to PPARα and PPARγ agonist activity using GAL4-LBD fusion constructs and GAL4-responsive Luciferase reporters in COS-1 cells. The oFA activity profile was compared with rosiglitazone and pirinixic acid (positive controls) and palmitic acid (negative control). Cytotoxicity was determined simultaneously assaying for lactate dehydrogenase (LDH) in the cell media. In addition, cytotoxicity was assessed using standard XTT assays. The dose-response curves are shown in Fig. 2 and summarized with corresponding EC_{50}-values in Table 1.

As can be seen both oFAs show an appreciable PPAR agonist dose-response, with EC_{50}-values in the micromolar range (Fig. 2; Table 1). At the same time the cell toxicity, as measured by lactate dehydrogenase leakage (LDH) and reduced metabolic NAD(P)H flux (XTT), is none to moderate in the same concentration range (10–30 μM). With respect to PPARα agonism, both **1** and **2** displayed EC_{50}-values and agonist activity comparable to pirinixic acid (WY-1464). However, when assaying **1** and **2** in the PPARγ activity assay, their EC_{50}-values were approximately 50 fold higher and their PPARγ agonist activities about 50% lower of that observed with rosiglitazone (BRL 49653; Fig. 2).

2.3. Selectivity

We next addressed the selectivity of the two oxo-fatty acids with respect to nuclear receptor agonist activity. To this end we transfected COS-1 cells with GAL4-LBD fusions of human PPARα, -δ, -γ, LXRα, -β, and RXRα, and treated them with increasing concentrations of the oFAs. Both natural products were able to activate PPARα and -γ in the range of 25–50 μM, while neither of them activated the LXRs or RXRα (Fig. 3). A small but significant PPARδ agonist activity was observed with 50 μM of **2**.

To be able to study the agonist activity of **1** and **2** in a more relevant context we expressed full-length human PPARα and −γ together with RXRα in COS-1 cells and assayed their transactivity on human *CPT1A*- and *PLIN1*-driven luciferase reporters in the presence or absence of the oxo-fatty acids. As can be seen in Fig. 4 both **1** and **2** were able to activate the PPARα-target gene promoter *CPT1A*, while only **1** activated the promoter of *PLIN1*, a *bona fide* PPARγ target gene. This activation was dependent of functional PPAR response elements (PPREs).

2.4. Activation of endogenous PPAR target genes

As both oxo-fatty acids displayed PPAR agonism *in vitro*, we asked whether **1** and **2** were able to activate fully chromatinized PPAR target genes in the human hepatocellular carcinoma cell line Huh7. Huh7 cells express both PPARα and −γ [31] (Ct: 26.3 and 24.6, respectively at baseline), but is often used in combination with PPARα agonist to assess regulation of liver-specific PPARα target genes. While both **1** and **2** were able to induce *CPT1A* and

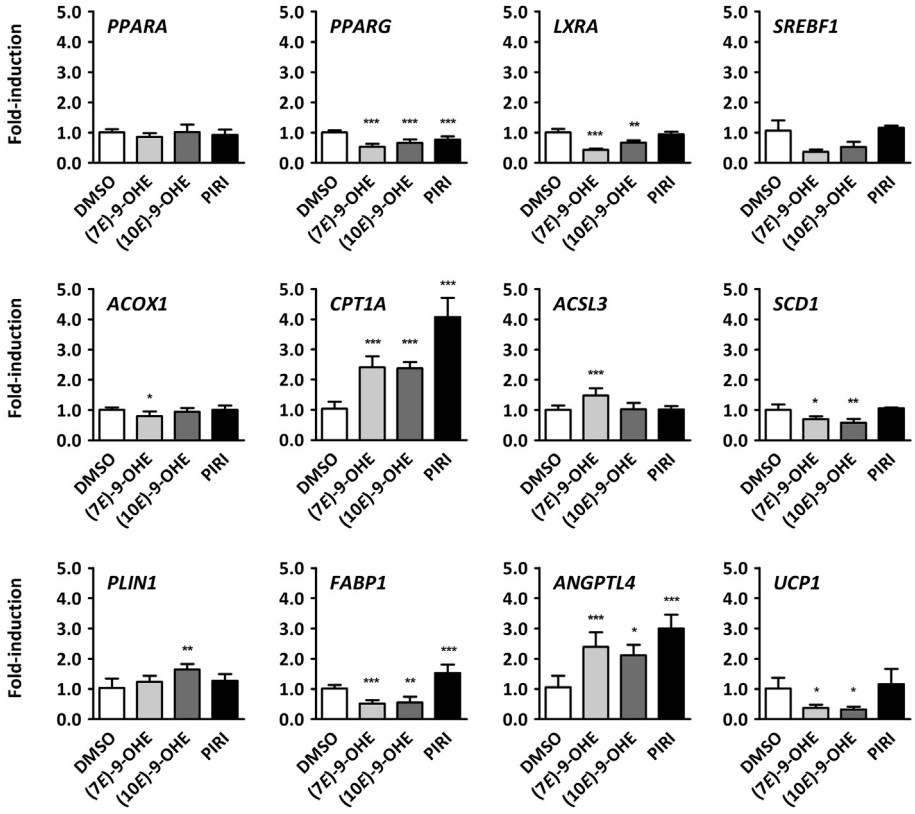

Fig. 5. The oxo-fatty acids 1 and 2 activate endogenous target genes in human hepatocarcinoma cells. Huh7 cells were stimulated with 50 μM of **1** (7*E*)-9-OHE, **2** (10*E*)-9-OHE or pirinixic acid (PIRI) for 24 h. Gene expression was analysed by qPCR using specific SYBR green primers. The results are shown as mean ± SEM. The data represent 3 biological replicates run in duplicates. *p < 0.05, **p < 0.01, ***p < 0.001.

ANGPTL4 expression, only **1** activated *ACSL3* (Fig. 5). *PLIN1* was only upregulated significantly by **2** but to very low levels. We were surprised to find that *ACOX1*, a classical PPARα target gene did not respond to any of the treatments. Several of the assayed target genes displayed a weak but significant downregulation (Fig. 5). Whether this was due to cytotoxic effects were not studied further.

2.5. Adipocyte differentiation

Turning our focus to adipocyte-specific target gene activation, we took advantage of the human Simpson-Golabi-Behmel syndrome (SGBS) pre-adipocyte cell line [32], and differentiated them into adipocytes using an 8 days differentiation protocol as described in the experimental section. On day 8 we either stimulated the cells with **1** or **2**, or rosiglitazone. As can be seen in Fig. 6 both **1** and **2** induce the expression of *CPT1A*, while only **2** was able to upregulate *ANGPTL4* expression. Oxo-fatty acid **1** and **2** were not able to induce classical adipocyte markers, such as *PLIN1*, *FABP4* and *ADIPOQ*. Even rosiglitazone failed to induce these genes any further. The reason for this is probably that differentiated SGBS cells already have a high expression of these genes. As an exception to this, *UCP1* was induced 10 times compared to baseline by rosiglitazone.

To address a potential role for **1** and **2** in adipocyte differentiation we compared the adipogenic potential of both compounds to rosiglitazone, by exchanging the classical PPARγ agonist with **1, 2** or DMSO the first 4 days of the differentiation protocol. On day 0, 4, 8 and 12 cells were either harvested for RNA isolation, to monitor the expression of target genes, or stained with Oil-Red-O to follow the inclusion of neutral lipids in lipid droplets.

Interestingly both **1** and **2** increased the number of cells with adipocyte-like, multilocular morphology, as well as the total volume of lipid droplets (no. of droplets × size). As expected, rosiglitazone was much more potent in inducing adipogenesis. Interestingly, the droplets formed during treatment with **1** seemed to be slightly bigger than the ones seen with rosiglitazone and **2** (Fig. 7, day 12). To evaluate the gene regulatory events underlying the morphological changes we assayed 20 genes relating to adipogenesis (Fig. 8), lipid storage and metabolism (Fig. 9) and adipokine signalling and browning (Fig. 10) using quantitative PCR. Both **1** and **2** were able to induce the classical adipogenic factors, *PPARG*, *CEBPA* and *CEBPB* (Fig. 8). The onset of the adipogenic gene program is also reflected in the upregulation of *PLIN1*, *FABP4*, *CD36* and *SCD1* which play important roles in fatty acid metabolism, transport and storage. This was seen with both oFAs (Fig. 9). However, the expression of most of these genes seem to be 5–10-fold lower on day 8–12 after stimulation with 25 μM **1** and **2** than with rosiglitazone. This might be related to what seems to be a transient induction of several important adipogenic driver genes when treating the cells with **1** and **2** (Fig. 8). Here gene expression peaked at day 4, while the rosiglitazone-treated cells were able to support a stable or increased expression of e.g. *PPARG* and *CEBPA* for the whole duration of the experiment. Part of the same pattern can be seen in Fig. 10 with the adipokines and thermogenic factors. Still, it should be noted that both **1** and **2** significantly upregulate the expression of adiponectin (*ADIPOQ*) and the mitochondrial brown fat uncoupling protein 1 (*UCP1*) over the 12 day differentiation period (Fig. 10).

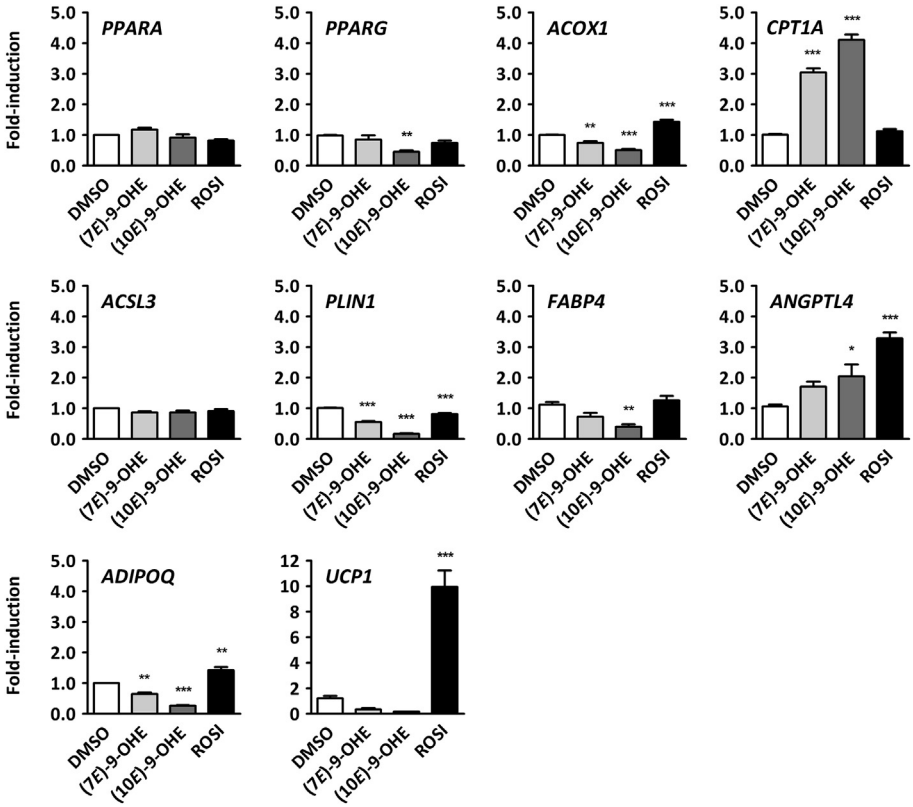

Fig. 6. The oxo-fatty acids 1 and 2 activate endogenous target genes in human adipocytes. SGBS cells were differentiated following standard protocol. On day eight the cells were stimulated with either 25 μM **1** (7*E*)-9-OHE, 25 μM **2** (10*E*)-9-OHE, or 2 μM rosiglitazone (ROSI) for 24 h. Gene expression was analysed by qPCR using specific SYBR green primers. The results are shown as mean ± SEM. The data represent three biological replicates run in duplicates. $^{*}p < 0.05$, $^{**}p < 0.01$, $^{***}p < 0.001$.

2.6. Adipocyte transcriptomics

To get a comprehensive view of the differential, transcriptional changes occurring during adipocyte differentiation, we sequenced RNA from SGBS cells differentiated for 8 days in medium supplemented with oxo-fatty acid **1**, **2** or rosiglitazone. Data from the treated cells were compared to SGBS cells at day 0. As can be seen from the Venn diagrams in Fig. 11A there was a significant overlap between the genes regulated by **1** and **2**, with 82.2% among the top 500 upregulated and 85.8% overlap among the top 500 downregulated genes. The overlap between rosiglitazone and the oxo-fatty acids was 42.0% and 58.4% for the same set of upregulated and downregulated genes, respectively. Pathway enrichment analysis made based on the KEGG collection displayed a significant overrepresentation of upregulated genes involved in e.g. PPAR signalling (hsa03320), fatty acid biosynthesis (hsa00061), and steroid biosynthesis (hsa00100) for **1** and **2**, as well as for rosiglitazone (Fig. 11B). Interestingly, biosynthesis of unsaturated fatty acids and fatty acid elongation (hsa00062 and hsa01041) seem to be overrepresented only in the rosiglitazone gene set. When analysing the downregulated genes, pathways such as extra cellular matrix-receptor interaction (hsa04512), TNF signalling (hsa04668), and AGE-RAGE signalling in diabetic complications (hsa04933) stood out (Fig. 11C). The principal component analysis made, based on the 8274 differentially expressed genes (DEGs) in our dataset showed that both oxo-fatty acid and rosiglitazone-treated cells differ significantly from the day 0 cells (Fig. 11D). Interestingly, the transcriptomes from oxo-fatty acid **1** cells cluster with the oxo-fatty acid **2** cells, and separate from the rosiglitazone transcriptomes when the total variance is explained using these principal components. Taking a closer look at the genes in the top tier enriched pathways (Fig. 12) the pattern from the differentiation experiments again becomes evident (Figs. 8–10). Even though both oFAs and rosiglitazone drive the expression of most genes in the sets in the same direction, the potency of **1** and **2** are lower, leading to a gradual decrease in expression and an earlier turning point from up-to downregulation (PPAR signalling) or vice versa (ECM-receptor interaction). The same is also seen for genes involved in fatty acid biosynthesis, adipokine signalling, biosynthesis of unsaturated fatty acids, and AGE-RAGE signalling in diabetic complications (Suppl. Fig. 1). In the pathway analysis shown in Fig. 12 and Suppl. Fig. 1, all genes in the KEGG gene set were included, independent of expression level. To get a better understanding of the difference between the rosiglitazone treated cells and the cells treated with **1** and **2**, we plotted the top 500 expressed genes in the rosiglitazone transcriptome in falling order and compared them to the same genes in the oFA transcriptomes (Fig. 13). Most of the genes express approximately 10-fold lower in the cells treated with **1** and **2**, resulting in the veil-like clustering below the rosiglitazone line. Interestingly, ten outliers are easily distinguishable for both treatments (Fig. 13; red circles).

A closer look at Table 2, listing these genes, shows that six out of seven overexpressed genes relate to extra cellular matrix. This probably reflects the more fibroblast-like properties of these cells, and indicates a restricted or delayed adipogenigenesis. The reduced levels of *PDK4* and *PDE3B* point in the same direction (Table 2). That being said, lower levels of phosphodiesterase 3 might be beneficial as this would lower the anti-lipolytic effect of insulin and enable full induction of *UCP1* expression and lipolysis in brown adipocytes in response to adrenergic stimulus [33,34].

Our data clearly show that while being able to activate both PPARα and PPARγ, oxo-fatty acids **1** and **2** have a reduced

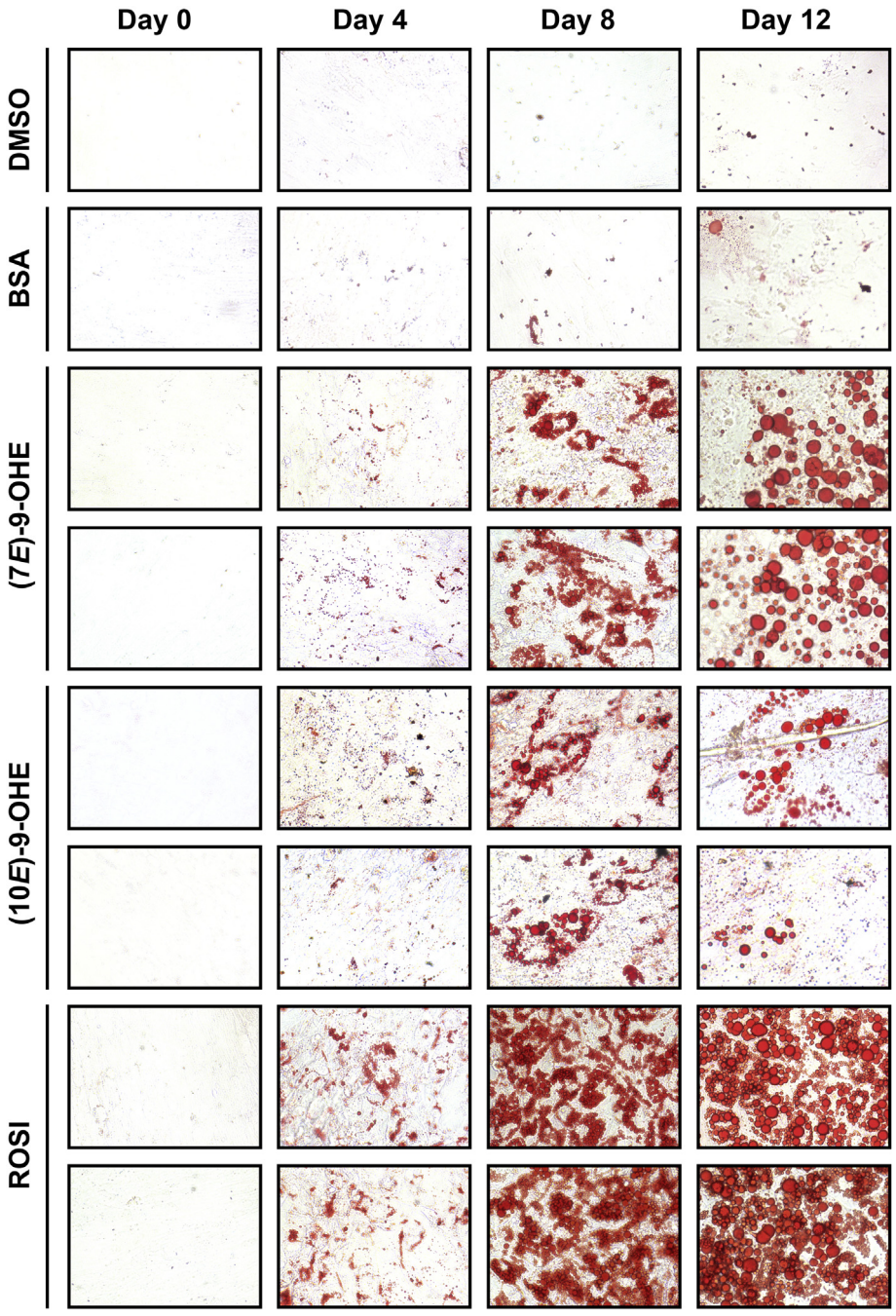

Fig. 7. The oxo-fatty acids 1 and 2 drive adipocyte differentiation, but to a lesser extent than rosiglitazone SGBS cells were differentiated in Quickdiff and 3FC medium for 4 and 8 days, respectively, following standard protocol. The quickdiff medium was supplemented with either 25 μM **1** (7*E*)-9-OHE, 25 μM **2** (10*E*)-9-OHE, or 2 μM rosiglitazone. DMSO (0.025%) and BSA (4.2 μM) were used as negative control. Adipocyte differentiation was monitored by staining of neutral lipids using Oil-Red-O. The images are representative for three biological replicates run in duplicates.

adipogenic effect compared to rosiglitazone. Even if we corrected for their lower potency by adding twice their EC_{50}-values in the stimulation- and differentiation cocktails, their reduced efficacy, especially with respect to PPARγ activity (Fig. 2), restricted gene activation and delayed adipogenigenesis (Figs. 7–10). This may at first glance be interpreted as a disadvantage. However, as many of the known side effects of the thiazolidinediones (TZDs) have been attributed to their potency and efficacy as classical PPARγ-specific agonists, this may in fact be an advantage. The strong adipogenic potential of the TZDs evidently contributes to the weight gain associated with the use of this of this type of anti-diabetic drugs [35,36]. While **1** and **2** are able to drive adipogenesis, their ability to activate target genes and support lipid storage in adipocytes is several fold lower than that of rosiglitazone (Figs. 7–9). Whether this is all due to reduced lipid synthesis or also reduced synthesis of lipid droplet coating factors, like the *PLIN* family (Fig. 14), is difficult to know.

The continuous increase in expression for many of the PPARγ target genes observed with TZD-stimulated adipogenesis (Figs. 9 and 10) has been reported in numerous papers, and is proposed to be caused by these agonists' ability to induce the biosynthesis of endogenous PPARγ ligands [37–39]. As unsaturated and elongated

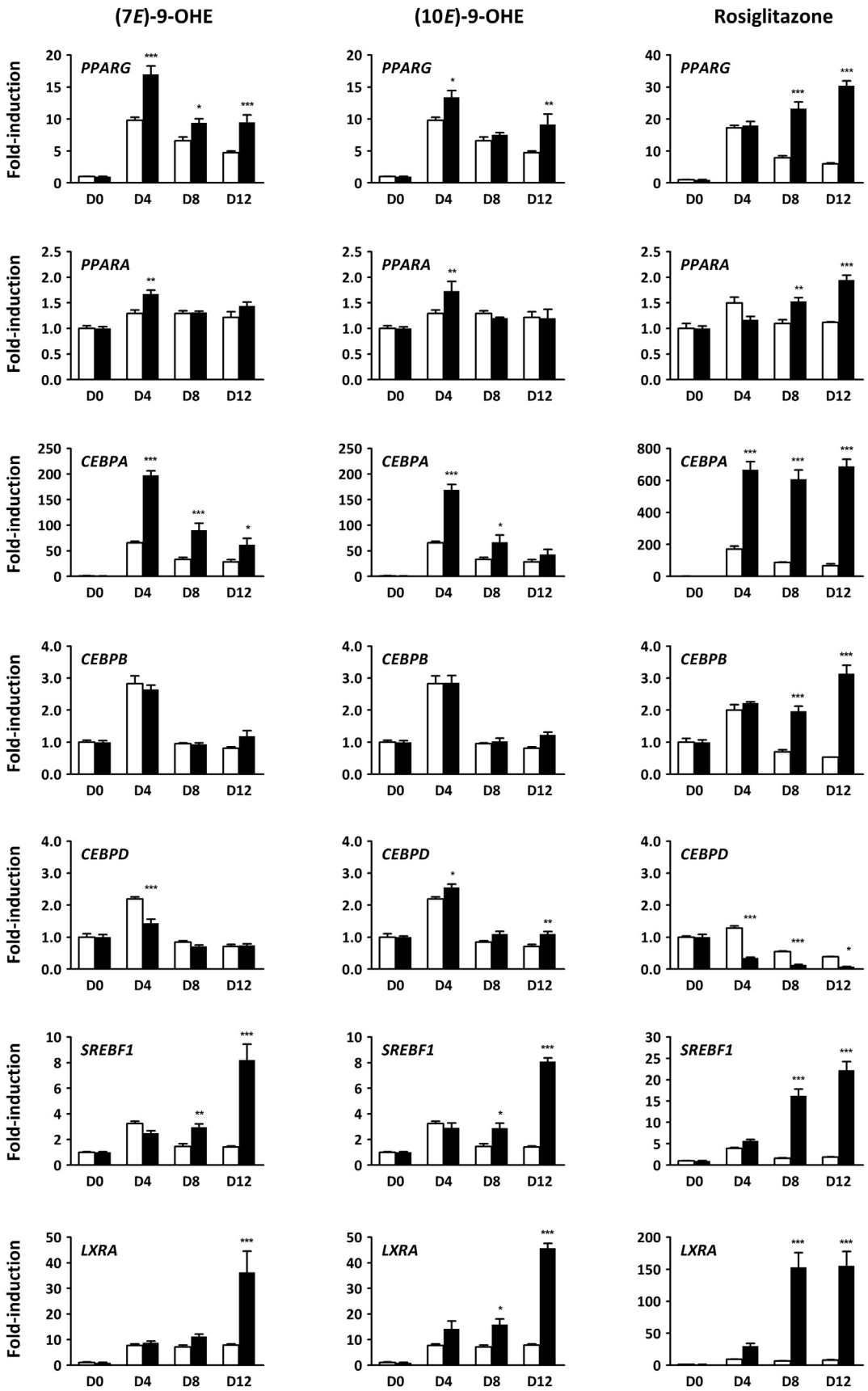

Fig. 8. The oxo-fatty acids 1 and 2 induce an adipogenic gene program in SGBS cells. SGBS cells were differentiated in Quickdiff and 3FC medium for 4 and 8 days, respectively, following standard protocol. The quickdiff medium was supplemented with either 25 μM **1** (7*E*)-9-OHE, 25 μM **2** (10*E*)-9-OHE, or 2 μM rosiglitazone. DMSO or DMSO:BSA were used as control. Gene expression was analysed by qPCR using specific SYBR green primers with RNA from cells harvested on day 0, 4, 8, and 12 (D0-D12). The results are shown as mean ± SEM. The data represent minimum 3 biological replicates run in duplicates. *$p < 0.05$, **$p < 0.01$, ***$p < 0.001$.

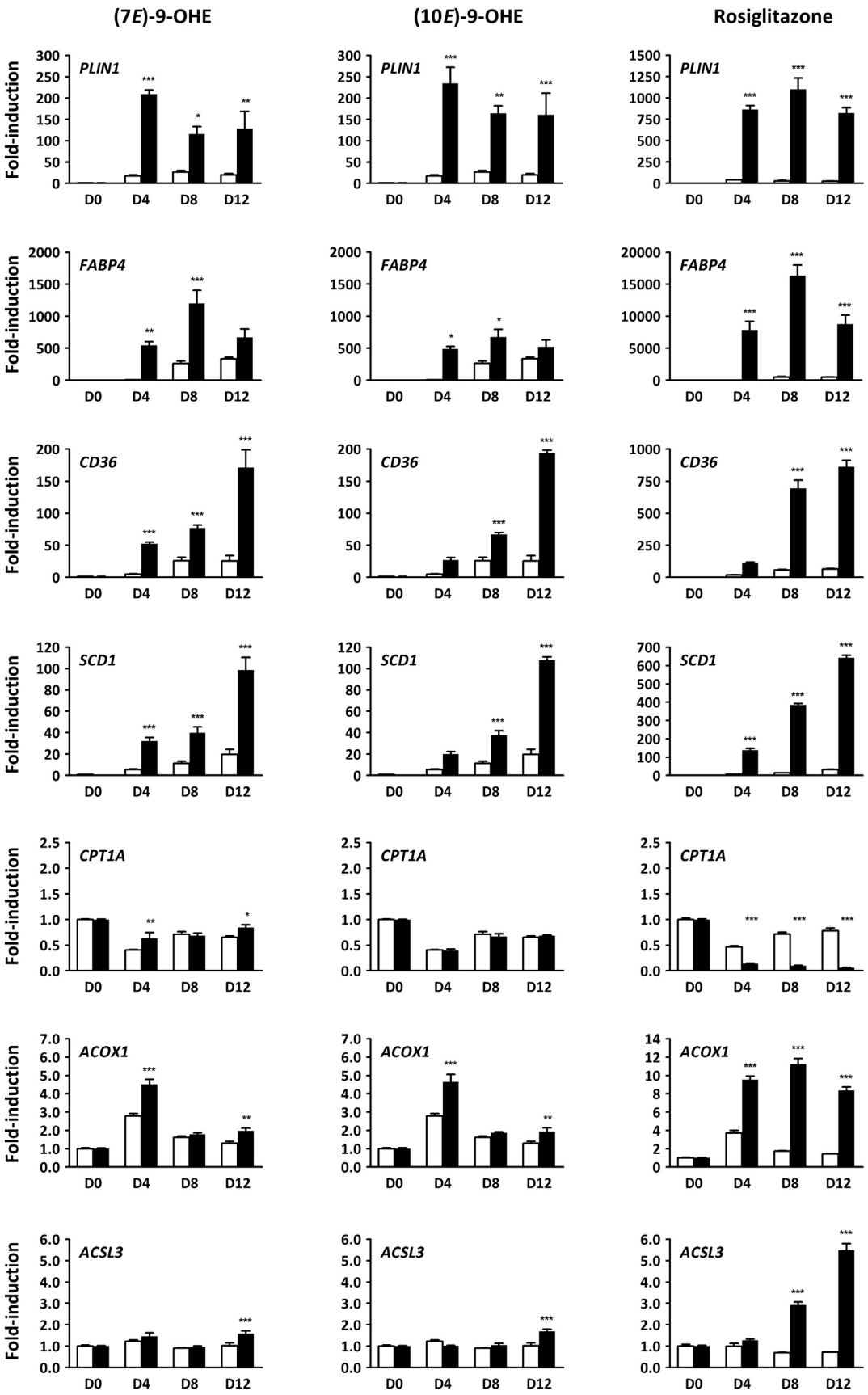

Fig. 9. The oxo-fatty acids 1 and 2 induce gene involved in lipid metabolism and storage in SGBS cells. SGBS cells were differentiated in Quickdiff and 3FC medium for 4 and 8 days, respectively, following standard protocol. The quickdiff medium was supplemented with either 25 μM **1** (7*E*)-9-OHE, 25 μM **2** (10*E*)-9-OHE, or 2 μM rosiglitazone. DMSO or DMSO:BSA were used as control. Gene expression was analysed by qPCR using specific SYBR green primers with RNA from cells harvested on day 0, 4, 8, and 12 (D0-D12). The results are shown as mean ± SEM. The data represent minimum three biological replicates run in duplicates. *$p < 0.05$, **$p < 0.01$, ***$p < 0.001$.

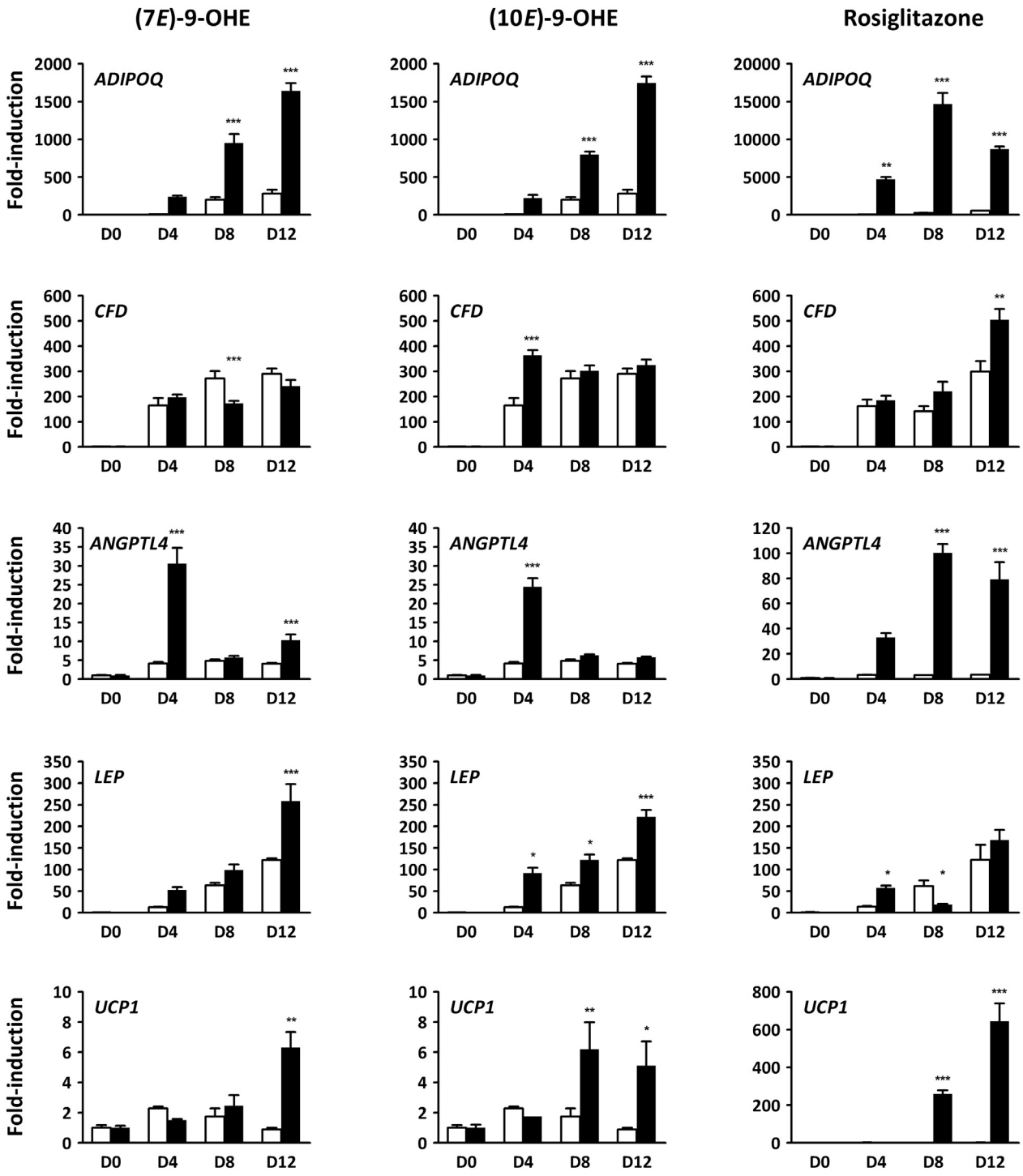

Fig. 10. The oxo-fatty acids 1 and 2 induce adipokines and browning factors. SGBS cells were differentiated in Quickdiff and 3FC medium for 4 and 8 days, respectively, following standard protocol. The quickdiff medium was supplemented with either 25 μM **1** (7*E*)-9-OHE, 25 μM **2** (10*E*)-9-OHE, or 2 μM rosiglitazone. DMSO or DMSO:BSA were used as control. Gene expression was analysed by qPCR using specific SYBR green primers with RNA from cells harvested on day 0, 4, 8, and 12 (D0-D12). The results are shown as mean ± SEM. The data represent minimum 3 biological replicates run in duplicates. $^{*}p < 0.05$, $^{**}p < 0.01$, $^{***}p < 0.001$.

carboxylic acids is the common chemical denominator of the many proposed endogenous PPAR ligands, e.g. PUFAs, prostaglandins and other oxidized eicosanoids, it is intriguing that two of the metabolic pathways necessary to produce such molecules (hsa00062: biosynthesis of unsaturated fatty acids; hsa01041fatty acid elongation) are underrepresented in the top tire DEGs from the oxo-fatty acid-stimulated cells (Fig. 11). The oxo-fatty acids, which structurally resemble the linoleic acid metabolites 9*S*-HODE and 13*S*-HODE [40], and even more so the corresponding oxo-fatty acids 9-oxo-ODE and 13-oxo-ODE [41], are still not able to support a PPAR-driven, self-reinforcing adipogenesis. Whether this is due to **1** and **2** not being able to bind covalently to PPARγ as other

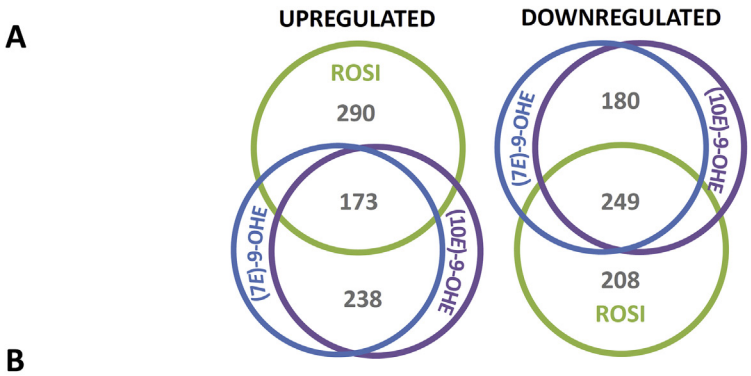

B

KEGG Pathway	Pathway ID	(7E) 9-OHE	(10E) 9-OHE	ROSI
Fatty acid elongation	hsa00062			
Biosynthesis of unsaturated fatty acids	hsa01040			
Steroid biosynthesis	hsa00100			
Fatty acid biosynthesis	hsa00061			
PPAR signaling pathway	hsa03320			
Fatty acid degradation	hsa00071			
Propanoate metabolism	hsa00640			
Terpenoid backbone biosynthesis	hsa00900			
Valine, leucine and isoleucine degradation	hsa00280			
Pyruvate metabolism	hsa00620			
Butanoate metabolism	hsa00650			
Citrate cycle (TCA cycle)	hsa00020			
beta-Alanine metabolism	hsa00410			
Glyoxylate and dicarboxylate metabolism	hsa00630			
Tyrosine metabolism	hsa00350			
Regulation of lipolysis in adipocytes	hsa04923			
Glycerolipid metabolism	hsa00561			
Fat digestion and absorption	hsa04975			
AMPK signaling pathway	hsa04152			
Glycolysis / Gluconeogenesis	hsa00010			
Peroxisome	hsa04146			
Adipocytokine signaling pathway	hsa04920			
Glycerophospholipid metabolism	hsa00564			
Insulin resistance	hsa04931			
Retinol metabolism	hsa00830			
Insulin signaling pathway	hsa04910			
Complement and coagulation cascades	hsa04610			
Longevity regulating pathway	hsa04211			
Phospholipase D signaling pathway	hsa04072			
Transcriptional misregulation in cancer	hsa05202			
Pathways in cancer	hsa05200			

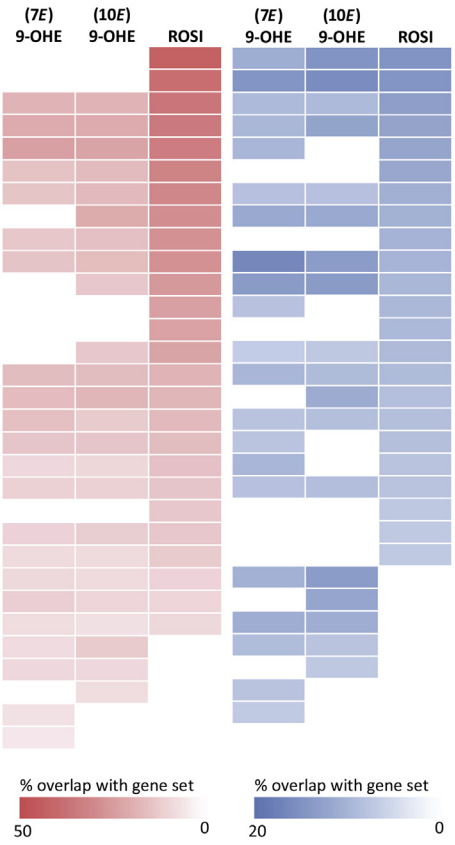

C

(7E) 9-OHE	(10E) 9-OHE	ROSI	Pathway ID	KEGG Pathway
			hsa04512	ECM-receptor interaction
			hsa04668	TNF signaling pathway
			hsa04933	AGE-RAGE signaling in diabetic complications
			hsa04510	Focal adhesion
			hsa04350	TGF-beta signaling pathway
			hsa04611	Platelet activation
			hsa04015	Rap1 signaling pathway
			hsa04610	Complement and coagulation cascades
			hsa04974	Protein digestion and absorption
			hsa04520	Adherens junction
			hsa04810	Regulation of actin cytoskeleton
			hsa04550	Signaling pathways reg. pluripotency of stem cells
			hsa04390	Hippo signaling pathway
			hsa04151	PI3K-Akt signaling pathway
			hsa04670	Leukocyte transendothelial migration
			hsa04640	Hematopoietic cell lineage
			hsa04621	NOD-like receptor signaling pathway
			hsa04068	FoxO signaling pathway
			hsa04380	Osteoclast differentiation
			hsa04060	Cytokine-cytokine receptor interaction
			hsa04022	cGMP-PKG signaling pathway
			hsa04014	Ras signaling pathway
			hsa04062	Chemokine signaling pathway
			hsa00330	Arginine and proline metabolism
			hsa00010	Glycolysis / Gluconeogenesis
			hsa04066	HIF-1 signaling pathway
			hsa04010	MAPK signaling pathway
			hsa04064	NF-kappa B signaling pathway
			hsa04145	Phagosome
			hsa04919	Thyroid hormone signaling pathway

D

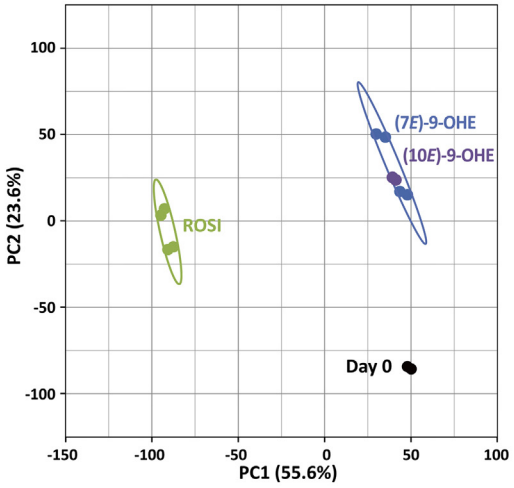

α,β-unsaturated ketones [41,42] or if it a stability issue, should be the focus of future structure-activity-relationship studies.

The reduced PPARγ agonistic activity of the oFAs is still strong enough to induce a robust expression of leptin (*LEP*) and the insulin-sensitizing adipokine adiponectin (*ADIPOQ*) in the adipocyte model (Fig. 10). At the same time their PPARα agonistic activity triggers fatty acid catabolism by inducing genes involved in β-oxidation, like *CPT1A* and *ACSL3* in hepatocytes (Fig. 5) and *CPT1A* in mature adipocytes (Fig. 6). This provides the oFAs with additional beneficial effects, known to be inherent properties of other PPARα/γ dual agonists [23,25,27,43]. Certain adipokines contribute to the development of obesity-associated insulin resistance, and studies on the link between obesity and insulin resistance have shown that there is an extensive crosstalk between adipocytes and immune cells in the adipose tissue (AT) [44,45]. Pro-inflammatory cytokines like IL-6, IL-1β and TNFα are mostly produced and secreted by macrophages infiltrating the AT. However as part of the crosstalk, macrophage-derived factors potently stimulate adipocytes to produce pro-inflammatory cytokines [46–48]. On the other side, activation of PPARγ by TZDs is shown to modulate this inflammatory-like state by suppressing cytokine production [49,50]. Thus, it is agreeable that TNF signaling (hsa04668) is one of the top three overrepresented pathways among the differentially downregulated genes (Fig. 11). As can be seen in Fig. 15, both oFAs and rosiglitazone are repressing cytokine production. Interestingly, IL-1β seems to be an exception: only **1** and **2** are able to repress the *IL1B* gene expression, while rosiglitazone seems to have no effect (Fig. 15). Since IL-1β is a major pro-inflammatory cytokine involved in AT metainflammation, and known to reduce adipose insulin sensitivity by downregulating *IRS1* and *GLUT4* expression [51,52], it is tempting to suggest that transcriptional regulation of this interleukin 1 B is another potential advantage of the oxo-fatty acids. Indeed *IRS2* expression increases with both **1** and **2**, while there is a tendency towards increased expression of *IRS1* and *SLC2A4 (GLUT4)* (Fig. 16).

The adverse effects reported with both PPARα-activating fibrates and PPARγ-activating thiazolidinedione, such as hepatotoxicity, pulmonary edema, myocardial infarction, weight gain, reduced bone density, and bladder and prostate cancer [15–22] were not addressed further in this paper. To proceed in this matter we would have to initiate *in vivo* studies in mice, which given the current *in vitro* cytotoxicity profile of **1** and **2** was not alternative. Certain of the reported side effects, like cancers of the bladder and prostate, is difficult to detect in animal models. Moreover, clinical trials are often too short to detect drug-related tumorigenesis. Therefore, the carcinogenic potential of most compounds is evaluated based on the extrapolation of minimum 2-year studies in rats or mice. Before testing the oFAs in long term *in vivo* experiments, less cytotoxic analogues would have to be synthesised and characterized.

3. Conclusion

Through the synthesis, pharmacological characterization, and biological evaluations of the oxo-fatty acids (7*E*)-9-oxohexadec-7-enoic acid (**1**) and (10*E*)-9-oxohexadec-10-enoic acid (**2**), we have shown that both compounds are semi-potent dual PPARα/γ agonists. While being derived from a marine alga, both oFAs regulate important PPAR target genes in human hepatocytes and adipocytes. Transcriptome analyses show that both compounds activate anti-diabetic gene programs in adipocytes by upregulating insulin-sensitizing adipokines and repressing pro-inflammatory cytokines. Simultaneously, they do not accumulate lipids in the adipocytes to the same extent as the classical thiazolidinediones. Together these features make the oxohexadecenoic acids interesting molecular scaffolds for designing new ligands with improved stability and a better toxicity profile to test in animal models relevant for T2D and metabolic syndrome.

4. Experimental section

4.1. Chemistry

4.1.1. Methyl 7-hydroxyheptanoate

Methyl 7-hydroxyheptanoate (**3**) was synthesized using literature protocols [28,29,53,54]. The physical and spectral data of **3** were in full agreement with those reported in the literature.

4.1.2. Methyl (E)-9-oxohexadec-7-enoate (**6**)

Phosphorane **5** (190 mg, 0.60 mmol, 1.18 equiv.) in THF (4 mL) was added *n*-BuLi (0.41 mL, 1.6 M in hexane, 1.30 equiv.) at −78 °C and stirred for 20 min. 1-Bromohexane (83 mg, 0.51 mmol, 1.00 equiv.) dissolved in CH_2Cl_2 (0.4 mL) was added dropwise and the solution was allowed to warm up to room temperature overnight. The reaction mixture was diluted with H_2O (10 mL) and extracted with CH_2Cl_2 (3 × 10 mL). The combined organic layers were dried (Na_2SO_4), before being concentrated *in vacuo*. The crude product was dissolved in CH_2Cl_2 (1.5 mL) and aldehyde **4** (80 mg, 0.51 mmol, 1.00 equiv.) in CH_2Cl_2 (1.0 mL) was added. The solution was stirred overnight before being concentrated *in vacuo*. The crude product was purified by column chromatography on silica (hexanes/EtOAc 9:1) to afford the title compound **6** as a colourless oil. Yield: 75 mg (53%). TLC (hexanes/EtOAc 9:1, $KMnO_4$ stain): $R_f = 0.12$; ^{1}H NMR (300 MHz, $CDCl_3$) δ 6.82 (dt, $J = 15.9$, 6.9 Hz, 1H), 6.10 (dt, $J = 15.9$, 1.5 Hz, 1H), 2.53 (t, $J = 7.4$, 2H), 2.33 (t, $J = 7.4$, 2H), 2.22 (td, $J = 7.5$, 1.5 Hz, 2H), 1.72–1.57 (m, 4H), 1.56–1.42 (m, 2H), 1.42–1.25 (m, 10H), 0.90 (t, $J = 6.6$, 3H); ^{13}C NMR (101 MHz, $CDCl_3$) δ 201.0, 174.2, 146.8, 130.6, 51.6, 40.4, 34.0, 32.3, 31.9, 29.4, 29.3, 28.8, 27.9, 24.8, 24.5, 22.8, 14.2. HRMS (TOF ES$^+$) Exact mass calculated for $C_{17}H_{30}NaO_3$ $[M+Na]^+$: 305.2092, found: 305.2102.

4.1.3. (E)-9-Oxohexadec-7-enoic acid (**1**)

The methyl ester **6** (20 mg, 0.07 mmol) was dissolved in phosphate buffer (pH = 7.2, 0.7 mL) and heated to 37 °C. Lipase from *Pseudomonas cepacia* (10 mg) was added and the reaction was stirred at ambient temperature for 24 h. The mixture was and extracted with CH_2Cl_2 (3 × 10 mL). The combined organic layers were dried (Na_2SO_4), before being concentrated *in vacuo*. The crude product was purified by column chromatography on silica (hexanes/EtOAc 97.5:2.5, then 90:10) to afford the title compound **1** as a white solid. Yield: 12 mg (64%). TLC (hexanes/EtOAc 7:3, $KMnO_4$ stain): $R_f = 0.12$; ^{1}H NMR (400 MHz, $CDCl_3$) δ 6.80 (dt, $J = 15.9$,

Fig. 11. Adipocyte transcriptomics. RNA from SGBS cells differentiated for 8 days in medium supplemented with either 25 μM **1** (7*E*)-9-OHE, 25 μM **2** (10*E*)-9-OHE or 2 μM rosiglitazone (all treatments n = 2–4), were sequenced on a Illumina NextSeq500, using strand-specific TruSeq RNA Sample Preparation, generating 2 × 75 bp paired-end reads. The reads were aligned, counted and normalized as Reads Per Kilobase of transcript per Million mapped reads (RPKM). **(A)** Venn diagrams of the top 500 up- or downregulated genes from the three treatments. **(B)** KEGG pathway enrichment analysis of the top 500 upregulated and **(C)** downregulated genes, relative to day 0, displayed in falling order based on percent overlap with the KEGG gene sets. Minimum overlap with input list: 3. p-value cutoff: $p < 0.01$. **(D)** Principal Component Analysis (PCA) of the 8274 DEGs in our dataset. Principal component 1 and 2 explains 55.6% and 23.6% of the total variance, respectively. Prediction ellipses represent the area for which a new observation from the same group will fall inside with a probability of 0.95.

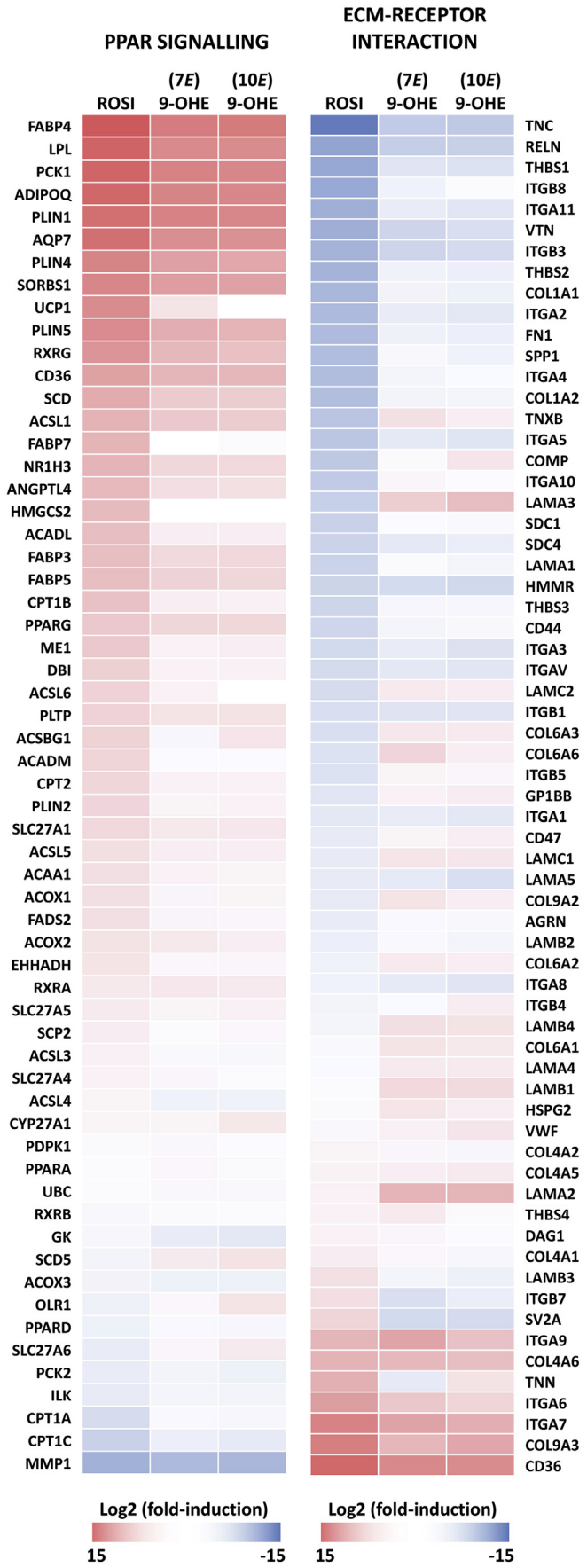

Fig. 12. The oxo-fatty acids 1 and 2 induce a transcriptional PPAR signalling program and downregulate genes involved in extra cellular matrix-receptor interaction. RNA sequencing data (RPKM) from SGBS cells differentiated for 8 days in medium supplemented with either 25 μM **1** (7*E*)-9-OHE, 25 μM **2** (10*E*)-9-OHE or 2 μM rosiglitazone (ROSI) (n = 2–4) were averaged and expressed as log2 fold-induction over unstimulated cells (day 0). Gene sets were grouped based on the Kyoto Encyclopedia of Genes and Genomes (KEGG).

6.9 Hz, 1H), 6.09 (d, J = 15.9 Hz, 1H), 2.52 (t, J = 7.5 Hz, 2H), 2.36 (t, J = 7.4 Hz, 2H), 2.22 (qd, J = 7.0, 1.5 Hz, 2H), 1.70–1.55 (m, 4H), 1.53–1.45 (m, 2H), 1.44–1.34 (m, 2H), 1.34–1.22 (m, 8H), 0.87 (t, J = 4.8, 3H); ^{13}C NMR (101 MHz, $CDCl_3$) δ 201.1, 178.6, 146.8, 130.6, 40.4, 33.8, 32.3, 31.9, 29.4, 29.3, 28.7, 27.9, 24.5, 24.5, 22.8, 14.2. HRMS (TOF ES$^+$) Exact mass calculated for $C_{16}H_{28}NaO_3$ $[M+Na]^+$: 291.1936, found: 291.1940.

4.1.4. ((8-Bromooctyl)oxy) (tert-butyl)dimethylsilane (**7**)

The compound **7** was prepared essentially as previously reported [30]. 8-Bromooctan-1-ol (6.00 mmol, 1.25 g) was dissolved in dry MeCN (12.0 mL) and added TBSCl (6.3 mmol, 0.94 g) and then imidazole (9.00 mmol, 0.630 g). The mixture was stirred under argon for 1 h. The mixture was filtered, evaporated, and purified by flash chromatography on silica gel (EtOAc:heptane, 49:1) to give the known compound **7** as a colourless oil. Yield 1.74 g (90%). ^{1}H NMR data was in agreement with literature [30]. ^{1}H NMR (400 MHz, Chloroform-*d*) δ 3.60 (t, J = 6.6 Hz, 2H), 3.41 (t, J = 6.9 Hz, 2H), 1.85 (quint., J = 6.9 Hz, 2H), 1.55–1.39 (m, 4H), 1.30 (m, 6H), 0.89 (s, 9H), 0.04 (s, 6H).

4.1.5. (*E*)-16-((Tert-butyldimethylsilyl)oxy)hexadec-6-en-8-ol (**8**)

Magnesium turnings (6.40 mmol, 0.154 g, 2.00 equiv.) and a magnet were placed in a flame dried round bottomed flask that was flushed with argon. A small amount of iodine (ca. 6 mg) was added. A solution of the bromide **7** (4.16 mmol, 1.34 g, 1.30 equiv.) in dry THF (12.0 mL) was prepared, and about 2 mL of this solution was quickly added to the magnesium turnings. After a few minutes of vigorous stirring, the reaction mixture went from clear brown to colourless. The remaining THF-solution of bromide **7** was then added over 5 min. After 1 h the solution was cloudy and the remaining magnesium was black. The mixture was cooled on an ice bath and added a solution of (*E*)-2-octenal (3.20 mmol, 0.403 g, 1.00 equiv.) in dry THF (4.00 mL) over 5 min. The cooling bath was removed and the mixture stirred for 1 h. After 1 h, the mixture was cooled on an ice bath and quenched with sat. aq. NH_4Cl (40 mL). The mixture was extracted with EtOAc (3 × 20 mL), dried ($MgSO_4$), evaporated and purified by flash chromatography on silica gel (EtOAc:heptane, 15:85) to give the desired product **8** as a colourless oil. Yield: 0.832 g (70%). R_f = 0.35 (EtOAc:heptane 3:7, $KMnO_4$-stain). ^{1}H NMR (400 MHz, Chloroform-*d*) δ 5.62 (m, 1H), 5.44 (broad dd, J = 15.4, 7.2, Hz, 1H), 4.02 (q, J = 6.7 Hz, 1H), 3.59 (t, J = 6.6 Hz, 2H), 2.07–1.95 (m, 2H), 1.59–1.22 (m, 21H), 0.89 (s, 9H), 0.88 (m, 3H), (0.04 (s, 6H). ^{13}C NMR (101 MHz, $CDCl_3$) δ 133.2, 132.4, 73.4, 63.5, 37.5, 33.0, 32.3, 31.5, 29.7, 29.7, 29.5, 29.0, 26.1 (3xC), 25.9, 25.6, 22.7, 18.5, 14.2, −5.1. Exact mass calculated for $C_{22}H_{46}O_2SiNa$ $[M+Na]^+$: 393.3159, found 393.3159.

4.1.6. (*E*)-9-((Tert-butyldimethylsilyl)oxy)hexadec-10-en-1-ol (**9**)

Step 1. Synthesis of (*E*)-5-(Hept-1-en-1-yl)-2,2,3,3,15,15,16,16-octamethyl-4,14-dioxa-3,15-disilaheptadecane. The alcohol **8** (2.18 mmol, 0.805 g, 1.00 equiv.) was dissolved in dry DMF (10.0 mL) and was added *tert*-butyl dimethylsilyl chloride (2.62 mmol, 0.394 g, 1.20 equiv.) and imidazole (5.45 mmol, 0.371 g, 2.50 equiv.). After stirring for 16 h, the mixture was added sat. aq. $NaHCO_3$ (30 mL) and water (50 mL), and the mixture was then extracted with EtOAc (3 × 30 mL), dried ($MgSO_4$) and evaporated. The residue

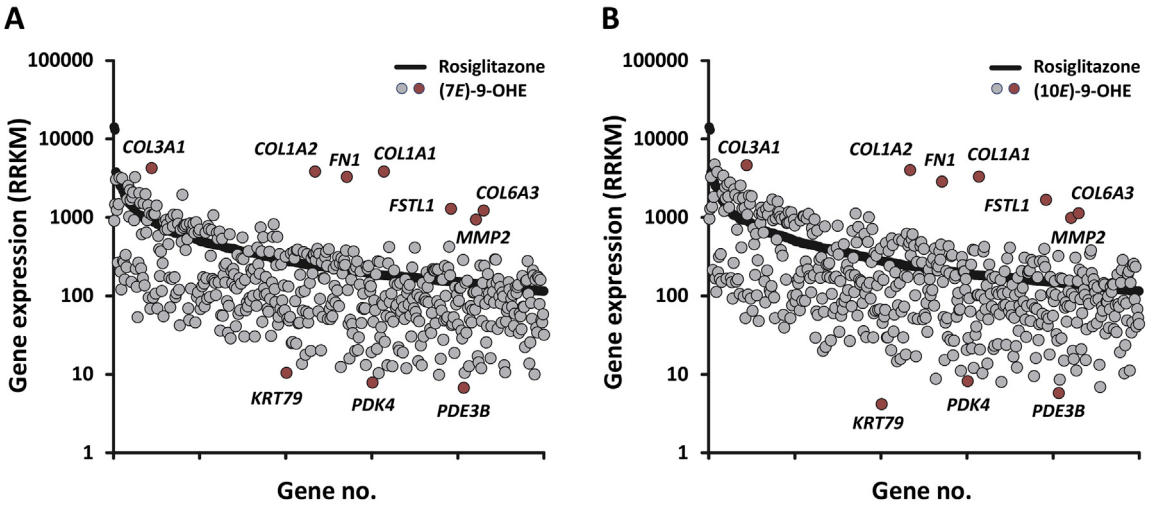

Fig. 13. The fatty acids 1 and 2 slow down fibroblast-to-adipocyte transition. Top 500 expressed genes in SGBS cells (day 8) differentiated in medium supplemented with rosiglitazone at was sorted in falling order based on RNA sequencing data (black line). The corresponding expression data from SGBS cells differentiated in medium supplemented with **1** (7*E*)-9-OHE (**A**) and **2** (10*E*)-9-OHE (**B**) was superimposed on the same graph (grey circles). Outliers are indicated with red circles and gene symbol.

Table 2
Outliers in the Top 500 expressed gene set.

Symbol	Gene name	Relative G.E.[a]
COL3A1	Collagen type III alpha 1 chain	+
COL1A2	Collagen type I alpha 2 chain	+
FN1	Fibronectin 1	+
COL1A1	Collagen type I alpha 1 chain	+
FSTL1	Follistatin like 1	+
MMP2	Matrix metallopeptidase 2	+
COL6A3	Collagen type VI alpha 3 chain	+
KRT79	Keratin 79	−
PDK4	Pyruvate dehydrogenase kinase 4	−
PDE3B	Phosphodiesterase 3 B	−

[a] Relative to rosiglitazone stimulated SGBS cells.

was purified by flash chromatography (EtOAc:heptane, 1:99) to give (*E*)-5-(Hept-1-en-1-yl)-2,2,3,3,15,15,16,16-octamethyl-4,14-dioxa-3,15-disilaheptadecane as a colourless oil. Yield: 0.960 g (91%). $R_f = 0.50$ (EtOAc:heptane 1:20, $KMnO_4$-stain). ^{1}H NMR (400 MHz, Chloroform-*d*) δ 5.49 (m, 6.6 Hz, 1H), 5.36 (dd, $J = 15.4$, 6.8, 1H), 4.00 (q, $J = 6.4$ Hz, 1H), 3.59 (t, $J = 6.6$ Hz, 2H), 1.99 (q, $J = 6.7$ Hz, 2H), 1.60–1.21 (m, 22H), 0.89 (d, $J = 4.4$ Hz, 21H), 0.05 (s, 6H), 0.04 (s, 3H), 0.02 (s, 3H). ^{13}C NMR (101 MHz, $CDCl_3$) δ 133.9, 130.5, 74.0, 63.5, 38.7, 33.0, 32.3, 31.5, 29.8, 29.7, 29.6, 29.1, 26.1 (3xC), 26.1 (3xC), 25.9, 25.6, 22.7, 18.5, 18.5, 14.2, −4.0, −4.6, −5.1 (2xC). Exact mass calculated for $C_{28}H_{60}O_2Si_2Na$ $[M+Na]^+$: 507.4024, found 507.4023.

Step 2. Protected (*E*)-5-(Hept-1-en-1-yl)-2,2,3,3,15,15,16,16-octamethyl-4,14-dioxa-3,15-disilaheptadecane (1,94 mmol,

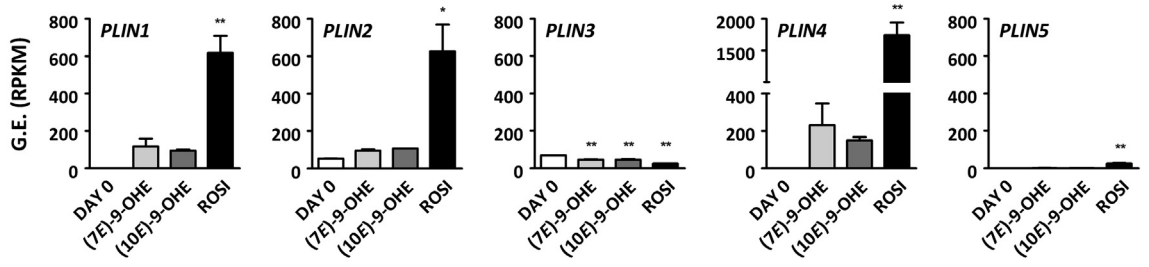

Fig. 14. Regulation of the lipid droplet-associated protein Perilipin family in SGBS cells. Comparison of gene expression (RPKM) of *PLIN1-5* from SGBS cells differentiated for 8 days in medium supplemented with either 25 μM **1** (7*E*)-9-OHE, 25 μM **2** (10*E*)-9-OHE, or 2 μM rosiglitazone. Gene expression at day 0 is included for comparison. The results are shown as mean ± SD, and represent 2-4 biological replicates. *p < 0.05, **p < 0.01.

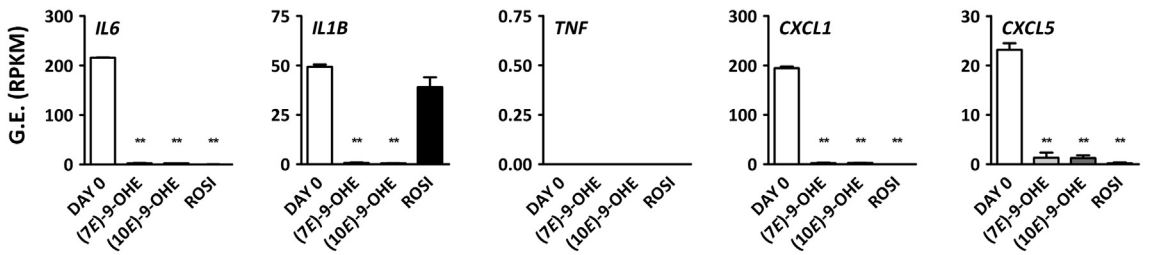

Fig. 15. The oxo-fatty acids 1 and 2 downregulate pro-inflammatory cytokines in SGBS cells. Comparison of gene expression (RPKM) of a selection of pro-inflammatory cytokines from SGBS cells differentiated for 8 days in medium supplemented with either 25 μM **1** (7*E*)-9-OHE, 25 μM **2** (10*E*)-9-OHE, or 2 μM rosiglitazone. Gene expression at day 0 is included for comparison. The results are shown as mean ± SD, and represent 2-4 biological replicates. **p < 0.01.

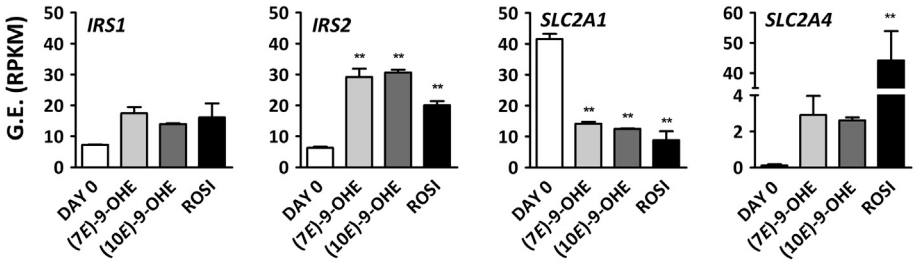

Fig. 16. Antidiabetic effects of oxo-fatty acids 1 and 2 in SGBS cells. Gene expression (RPKM) of insulin receptor substrates *IRS1* and *IRS2* and the glucose transporters *SLC2A1* and *SLC2A4* were measured as proxies for increased insulin sensitivity and glucose uptake in SGBS cells differentiated for 8 days in medium supplemented with either 25 μM **1** (7*E*)-9-OHE, 25 μM **2** (10*E*)-9-OHE, or 2 μM rosiglitazone. Gene expression at day 0 is included for comparison. The results are shown as mean ± SD, and represent 2-4 biological replicates. $^{**}p < 0.01$.

0,942 g) was dissolved in THF (28 mL) and added a mixture of trifluoroacetic acid in water (4.5 mL, TFA:H_2O 1:9). The mixture was stirred at ambient temperature for 3 h before it was quenched by addition of sat. aq. $NaHCO_3$ (50 mL). The mixture was extracted with EtOAc (3 × 30 mL). The combined organic layer was washed with sat. aq. $NaHCO_3$ (3 × 10 mL) and brine (1 × 10 mL), dried ($MgSO_4$) and evaporated. The residue was purified by flash chromatography (EtOAc:heptane 1:9) to yield the primary alcohol **9** as a colourless oil. Yield: 0.467 g (65%). $R_f = 0.35$ (EtOAc:heptane 3:7, $KMnO_4$-stain). ^{1}H NMR (400 MHz, $CDCl_3$) δ 5.54–5.44 (m, 1H), 5.36 (broad dd, $J = 15.3$, 6.8, 1H), 4.00 (q, $J = 6.4$ Hz, 1H), 3.63 (t, $J = 6.6$ Hz, 2H), 1.98 (q, $J = 7.9$, 7.4 Hz, 2H), 1.60–1.52 (m, 2H), 1.52–1.21 (m, 20H), 0.92–0.84 (m, 3H), 0.88 (s, 9H), 0.03 (s, 3H), 0.01 (s, 3H). ^{13}C NMR (101 MHz, $CDCl_3$) δ 133.9, 130.5, 74.0, 63.2, 38.7, 32.9, 32.2, 31.5, 29.7, 29.7, 29.5, 29.1, 26.1 (3xC), 25.9, 25.6, 22.7, 18.4, 14.2, −4.0, −4.6. Exact mass calculated for $C_{22}H_{46}O_2SiNa$ $[M+Na]^+$: 393.3159, found 393.3159.

4.1.7. (E)-9-Hydroxyhexadec-10-enoic acid (**10**)

Alcohol **9** (1.53 mmol, 0.566 g, 1.00 equiv.) was dissolved in CH_2Cl_2 (15.0 mL) and added $NaHCO_3$ (0.39 g, 3.00 mmol) and Dess-Martin Periodinane (1.84 mmol, 0.780 g, 1.2 equiv.). The mixture was stirred at room temperature for 1.5 h and then filtered through a plug of silica gel that was washed with a small amount of EtOAc:heptane (1:4). The residue was dissolved in MeCN (15.0 mL) and 2-methyl-2-butene (3.60 mL). Then a solution of NaH_2PO_4 (6.00 mmol, 0.722 g, 7.00 equiv.) in water (6.00 mL) was added. Finally, 80% $NaClO_2$ (7.74 mmol, 0.872 g, 9.00 equiv.) was added and the mixture was stirred vigorously for 80 min. Then sat. aq. NaH_2PO_4 (50 mL) was added and the mixture was extracted with EtOAc (3 × 20 mL). The combined organic extracts were washed with water (1 × 10 mL), dried (Na_2SO_4) and evaporated. The resulting residue was taken through a short plug of silica gel eluting with CH_2Cl_2:MeOH (19:1). The residue was dissolved in dry THF (5.0 mL) and added a solution of TBAF (10.0 mL, 1.0 M in THF) at 0 °C. The mixture was stirred at room temperature overnight. Sat. aq. NaH_2PO_4 (50 mL) was added and the mixture was extracted with EtOAc (2 × 30 mL). The combined organic layers were washed with brine, dried (Na_2SO_4) and evaporated. The residue was purified by flash chromatography using a gradient of 5–70% EtOAc in heptane to afford the desired product **10** as a colourless wax. Yield: 156 mg (67%). $R_f = 0.46$ (DCM:MeOH:AcOH 20:1:0.1, $KMnO_4$-stain). ^{1}H NMR (400 MHz, $CDCl_3$) δ 5.69–5.57 (m, 1H), 5.44 (ddt, $J = 15.3$, 7.2, 1.4 Hz, 1H), 4.03 (q, $J = 6.7$ Hz, 1H), 2.33 (t, $J = 7.5$ Hz, 2H), 2.01 (q, $J = 6.9$, 2H), 1.70–1.42 (m, 4H), 1.42–1.20 (m, 15H), 0.88 (t, $J = 6.9$ Hz, 3H). ^{13}C NMR (101 MHz, $CDCl_3$) δ 179.6, 133.0, 132.5, 73.4, 33.7, 34.6, 32.3, 31.5, 29.5, 29.3, 29.3, 29.1, 29.0, 25.5, 24.8, 22.7, 14.2. Exact mass calculated for $C_{16}H_{30}O_3Na$ $[M+Na]^+$: 293.2087, found 293.2088.

4.1.8. (E)-9-Oxohexadec-10-enoic acid (**2**)

Alcohol **10** (79 mg, 0.30 mmol) was dissolved in dry CH_2Cl_2 (20 mL) and added celite (600 mg), MnO_2 (85%, 4.4 mmol, 450 mg) and the resulting mixture was stirred 20 h at room temperature. The mixture was filtered through a plug of celite that was washed with EtOAc. The filtrate was evaporated and purified by column chromatography on silica gel (heptane/EtOAc 70:30, then 60:40) to afford the title compound **2** as a pale yellow wax. Yield: 12 mg (15%). $R_f = 0.34$ (CH_2Cl_2/MeOH/AcOH 20:1:0.1, CAM stain). ^{1}H NMR (400 MHz, $CDCl_3$) δ 6.82 (dt, $J = 15.8$, 6.9 Hz, 1H), 6.08 (dt, $J = 15.7$, 1.5 Hz, 1H), 2.52 (t, $J = 7.4$ Hz, 2H), 2.34 (t, $J = 7.5$ Hz, 2H), 2.20 (qd, $J = 7.0$, 1.5 Hz, 2H), 1.61 (m, 4H), 1.45 (m, 2H), 1.37–1.28 (m, 10H), 0.91–0.87 (t, $J = 6,8$ Hz, 3H). ^{13}C NMR (101 MHz, $CDCl_3$) δ 201.1, 178.6, 147.6, 130.4, 40.1, 33.9, 32.6, 31.5, 29.23, 3.19, 29.0, 27.9, 24.8, 24.3, 22.6, 14.1. Exact mass calculated for $C_{16}H_{28}O_3Na$ $[M+Na]^+$: 291.1931, found 291.1930.

4.2. Biology

4.2.1. Plasmids

The pSG5-Gal4-hPPARα-LBD, pSG5-Gal4-hPPARδ-LBD, and pSG5-Gal4-hPPARγ-LBD encoding Gal4 DNA-binding domain (DBD; aa 1-147) fused in frame with the SV40 nuclear localization signal 1 (NLS1), and ligand binding domain (LBD) of human PPARα (aa 168-468), PPARδ (aa 140-441), and PPARγ (aa 205-505) has been described earlier [14]. pSG-Gal4 encoding Gal4 DBD and SV40 NLS1 was made by amplifying this part of the pSG5-Gal4-hPPARδ-LBD, using a custom-made reverse primer that made up the original multi cloning site (MCS): KpnI-XmaI-NotI-EagI-SacII-BamHI-BglII. This PCR product was then subcloned between XhoI and BamHI in pSG5-Gal4-hPPARδ-LBD, exchanging PPARδ-LBD with the new MCS. pSG5-Gal4-hLXRα-LBD, pSG5-Gal4-hLXRβ-LBD, and pSG5-Gal4-hRXRα-LBD encoding Gal4 DBD, SV40 NLS1, and the LBDs of human LXRα (aa 164-447), LXRβ (aa 155-461), and RXRα (aa 202-462) were made by PCR amplifying the respective LBDs and subcloning them into pSG-Gal4 between KpnI and BamHI (LXRα and -β) or KpnI and SacII (RXRα). The plasmids encoding FLAG-tagged full-length human PPARα, PPARγ, and RXRα have been described earlier [14,55]. The pGL3-5 × UAS-SV40 luciferase reporter, as well as the human *PLIN1*-driven reporters, pGL3-hPLIN1-3′del and pGL3-hPLIN1-3′del PPREmut, have been described before [9,14]. The human *CPT1A*-driven reporters, pGL3-hCPT1AInt and pGL3-hCPT1AInt PPREmut, were received as a gift from Prof. Diego Haro Bautista and have been described previously [56]. The vector pRL-CMV (Promega, Madison, WI), constitutively expressing Renilla Luciferase, was used as a control of transfection efficiency. All cloned plasmids have been sequenced. Cloning primer sequences are available upon request.

4.2.2. Cell culture, transfection and luciferase assays

COS-1 cells (ATCC® CRL-1650) were maintained in Dulbecco's modified Eagle's medium (DMEM; D6546, Sigma-Aldrich, St. Louis, MO) containing penicillin/streptomycin (50 U/mL; 50 μg/mL), 4 mM L-glutamine, and 10% fetal bovine serum (F7524; Sigma-Aldrich), at 37 °C in a humidified atmosphere of 5% CO_2 in air. Cell confluence never exceeded 80% before subculturing or transfection. For the dose-response and specificity assays, COS-1 cells were seeded at 7×10^4 cells/well in 24-well plates. After 24 h cells were transfected with either 0.1 μg of the Gal4-DBD-NR-LBD expression plasmids, 0.2 μg of the 5 × UAS-SV40 luciferase reporter, and 0.05 μg of the Renilla Luciferase-coding internal control (pRL-CMV), or 0.2 μg of the full-length PPAR and RXR-expressing plasmids, together with 0.2 μg of any of the *PLIN1*- or *CPT1A*-driven reporters, and 0.05 μg of pRL-CMV using Lipofectamin 2000 (Life Technologies, Carlsbad, CA). After 5 h the cells were treated with (7*E*)-9-oxohexadec-7-enoic acid, (10*E*)-9-oxohexadec-10-enoic acid, pirinixic acid (WY-14643; C7081, Sigma-Aldrich), PPARγ: rosiglitazone (BRL-49653; Cayman Chemical, Ann Arbor, MI), or palmitic acid (C16:0; P0500, Sigma-Aldrich) in DMSO (final conc. 0.1%). After 18 h cells were washed in PBS and lysed in Passive Lysis Buffer (Promega, Madison, WI) and Dual-Luciferase® ReporterAssay System (Promega) was run on a Synergy 2 plate reader (BioTek® Instruments, Winooski, VT) following the manufacturers protocol. The Firefly Luciferase readings were normalized to the Renilla Luciferase numbers and data from at least three independent transfection experiments run in quadruplicate are presented.

Huh-7 human hepatoma cells were maintained in DMEM (D6546, Sigma-Aldrich) containing penicillin/streptomycin (50 U/mL; 50 μg/mL), 4 mM L-glutamine, 10% fetal bovine serum (F7524; Sigma-Aldrich), and 0.1% ITS (insulin/transferrin/sodium selenite; I3146, Sigma-Aldrich), at 37 °C in a humidified atmosphere of 5% CO_2 in air. Cell confluence never exceeded 80% before subculturing or transfection. The cells were seeded at 2×10^5 cells/well in 12-well plates. After 24 h cells were treated with 50 μM (7*E*)-9-oxohexadec-7-enoic acid, (10*E*)-9-oxohexadec-10-enoic acid, or pirinixic acid in DMSO (final conc. 0.1%). On the day after the cells were washed and scraped in RLT buffer (Qiagen, Hilden, Germany).

Human Simpson-Golabi-Behmel syndrome (SGBS) cells were cultured and differentiated into adipocytes essentially as described [32]. Briefly, cells were maintained in basal medium (DMEM/nutrient mix F-12; D6421, Sigma-Aldrich) supplemented with 2 mg/L of biotin, 1 mg/L of D-pantothenate, 4 mM L-glutamine, penicillin/streptomycin (50 U/mL; 50 μg/mL), and 10% non-inactivated fetal calf serum (F7524; Sigma-Aldrich). For adipocyte differentiation, cells were seeded at low passage (P6-P8) at 0.8×10^5 cells/well in 12-well plates and grown to confluence (day 0). From day 0 to day 4 the cells were exposed to adipogenic medium (Quickdiff; 3FC supplemented with 25 nM dexamethazone, 0.5 mM isobutylmethylxanthine, and 2 μM rosiglitazone, 25 μM **1** (7*E*)-9-OHE:BSA, or 25 μM **2** (10*E*)-9-OHE:BSA, followed by continuous culturing in 3FC (basal medium supplemented with 10 μg/mL human transferrin, 20 nM human insulin, 100 nM cortisol, and 0.2 nM triiodothyronine). Medium was renewed every fourth day. In a set of separate experiments SGBS cells were differentiated with Quickdiff medium, including 2 μM rosiglitazone, from day 0 to day4. Then at day 8 the cells were stimulated with 25 μM **1** (7*E*)-9-OHE:BSA, 25 μM **2** (10*E*)-9-OHE:BSA, or 2 μM rosiglitazone in 3FC medium for 24 h.

4.2.3. Cytotoxicity assays

The cytotoxic effect of the compounds were evaluated in COS-1 cells, using the Roche Cytotoxicity Detection Kit (#1164479300, Sigma-Aldrich) measuring lactate dehydrogenase (LDH) leaked from the cells or by the XTT-based In Vitro Toxicology Assay Kit (#TOX2-1 KT, Sigma-Aldrich) measuring reduced metabolic NAD(P)H flux. Both assays were run as described by the company, and absorbance were read at 492/750 nm and 450/690 nm for the LDH and XTT assay, respectively, on a Synergy H1 Hybrid Multi-Mode Microplate Reader (BioTek® Instruments).

4.2.4. Staining of lipids

SGBS cells were washed in PBS, fixed in 4% paraformaldehyde/PBS for 15 min, washed with PBS, and incubated with Oil Red O for 15 min to stain neutral lipids. Finally, the cells were washed in PBS to remove excess dye. After staining, the cells were visualized through 10× and 40× objectives on an Olympus CKX41 inverted microscope (Olympus, Hamburg, Germany). Images were captured with a ColorView IIIu light microscope CCD camera (Olympus) operated by cell* imaging software v.3.4 (Olympus). Images were processed with Adobe Photoshop CS6 (Adobe Systems Inc. San Jose California, USA).

4.2.5. RNA extraction, cDNA synthesis and real-time quantitative PCR (qPCR)

RNA was isolated using the RNeasy Mini kit (#74104, Qiagen) with the following modifications: Lysates from cells with high-fat content, such as SGBS cells on day 8 and 12, were mixed 1:1 in 70% ethanol in high salt solution (0.45 M NaCl/0.24 M Na-acetate), before applied to the columns. Isolated RNA (500 ng) was reverse transcribed into cDNA using SuperScript III Reverse Transcriptase (Invitrogen, Thermo Fisher Scientific, Waltham, MA, USA) and random hexamer primers. qPCR was performed with 2.5 μL cDNA, equivalent to 12.5 ng RNA, in a 10 μL reaction mix using Kapa SYBR FAST qPCR Master Mix (KapaBiosystems, Roche, Basel, Switzerland) on a Bio-Rad CFX96 Touch™ Real-Time PCR Detection System. Gene expression was normalized against the expression of TATA-binding protein (*TBP*). Assay primers were designed with Primer-BLAST software (NCBI, Bethesda, MD, USA) [57]. Primer sequences are listed in Suppl. Table S1.

4.2.6. RNA-sequencing

SGBS cells were differentiated in Quickdiff and 3FC medium for 4 plus 4 days, respectively, following the protocol described above. The Quickdiff media was supplemented with either 2 μM rosiglitazone (n = 4), 25 μM **1** (7*E*)-9-OHE:BSA (n = 4), or 25 μM **2** (10*E*)-9-OHE:BSA (n = 2). Undifferentiated SGBS cells, grown to confluence (day 0), were also assayed (n = 2). The SGBS cells were lysed in RTL buffer and total RNA extracted using RNeasy Mini kit (Qiagen). RNA quality was assessed on a BioAnalyzer 2100, using the Agilent RNA 6000 Nano Kit (#5067-1511; Agilent Technologies Inc, Santa Clara, CA). The RIN values (RNA integrity number) varied between 9.80 and 10.00, with an average of 9.95. Illumina sequencing libraries were prepared according to the strand-specific TruSeq RNA Sample Preparation Guide (revision D) and sequencing performed on a NextSeq 500 (Illumina, San Diego, CA), using v2 reagents. Libraries were sequenced using 2 × 75 bp paired-end reads. For pre-alignment quality control, we used the software FastQC v0.10.1. The mean library size was ~18 million read pairs, with no difference between groups or time points. Alignment of cDNA sequenced reads was done using Tophat v2.0.8, Samtools v0.1.18, and Bowtie v2.1.0 with default settings against the UCSC hg19 annotated transcriptome and genome. Reads were counted by Cufflinks v2.1.1 and presented as Reads Per Kilobase of transcript per Million mapped reads (RPKM). Differentially expressed genes were identified using one-way anova and an RPKM cut-off set to 5.

4.2.7. Accession number

Accession number for the RNA-seq data reported in this article is NCBI GEO GSE115827.

4.2.8. Statistical analysis

Statistical analyses were performed using GraphPad Prism 6 (GraphPad Software Inc., San Diego, CA, USA). All data are presented as mean and standard error of the mean (SEM) or standard deviation (SD). Statistical differences between groups were determined by two-way analysis of variance (ANOVA) followed by Tukey's multiple comparison tests. For all statistical tests $p < 0.05$ was considered statistically. Any exceptions to this are given in the Figure legends.

4.2.9. Venn diagrams

Top 500 differentially expressed genes in our dataset, using mean of replicates, were visualized using the Venn diagram drawing tool from Bioinformatics & Evolutionary Genomics, Ghent University, Belgium (http://bioinformatics.psb.ugent.be/webtools/Venn).

4.2.10. Principal component analysis

Principal component analysis (PCA) of the 8274 differentially expressed genes in our dataset was made with Clustvis, a web tool for visualizing clustering of multivariate data (https://biit.cs.ut.ee/clustvis) [58]. Row scaling was made by unit variance scaling (UVS) and missing data imputation was made using singular value decomposition (SVD).

4.2.11. Pathway enrichment analysis

Pathway enrichment analysis of the top 500 differentially up- and downregulated genes, using mean of replicates, were made with the ConsensusPathDB tool from the Max-Planck-Institute for Molecular Genetics (http://cpdb.molgen.mpg.de) [59], using the Kyoto Encyclopedia of Genes and Genomes (KEGG) gene sets v80.0, pathway ID: 00000-05000 excluding non-relevant human diseases. Minimum overlap with input list was set to 3 and the p-value cutoff to $p < 0.01$.

Notes

The authors declare no competing financial interest.

Acknowledgements

The Norwegian Research Council is gratefully acknowledged for generous funding to T.S and S.M.P (BIOTEK 2021 208452/010) and T.V.H (FRIPRO-FRINATEK 230470). The authors would like to thank Christin Lucas for excellent technical assistance, and Angel Moldes-Anaya, Sindre Lee-Ødegård, and members of the Nebb and Hansen labs for scientific discussions. Finally, we are grateful to Krister Bamberg and Diego Haro Bautista for providing us with plasmids.

Appendix A. Supplementary data

Supplementary data related to this article can be found at https://doi.org/10.1016/j.ejmech.2018.06.034.

References

[1] WHO, Obesity and overweight, WHO Fact. sheet 311 (2013).
[2] W. Wahli, L. Michalik, PPARs at the crossroads of lipid signaling and inflammation, Trends Endocrinol. Metabol.: TEM (Trends Endocrinol. Metab.) 23 (2012) 351–363.
[3] L. Nagy, H.Y. Kao, D. Chakravarti, R.J. Lin, C.A. Hassig, D.E. Ayer, S.L. Schreiber, R.M. Evans, Nuclear receptor repression mediated by a complex containing SMRT, mSin3A, and histone deacetylase, Cell 89 (1997) 373–380.
[4] V. Perissi, M.G. Rosenfeld, Controlling nuclear receptors: the circular logic of cofactor cycles, Nat. Rev. Mol. Cell Biol. 6 (2005) 542–554.
[5] P. Puigserver, G. Adelmant, Z. Wu, M. Fan, J. Xu, B. O'Malley, B.M. Spiegelman, Activation of PPARgamma coactivator-1 through transcription factor docking, Science 286 (1999) 1368–1371.
[6] D. Auboeuf, J. Rieusset, L. Fajas, P. Vallier, V. Frering, J.P. Riou, B. Staels, J. Auwerx, M. Laville, H. Vidal, Tissue distribution and quantification of the expression of mRNAs of peroxisome proliferator-activated receptors and liver X receptor-alpha in humans: no alteration in adipose tissue of obese and NIDDM patients, Diabetes 46 (1997) 1319–1327.
[7] P. Ferre, The biology of peroxisome proliferator-activated receptors: relationship with lipid metabolism and insulin sensitivity, Diabetes 53 (Suppl 1) (2004) S43–S50.
[8] A. Chawla, E.J. Schwarz, D.D. Dimaculangan, M.A. Lazar, Peroxisome proliferator-activated receptor (PPAR) gamma: adipose-predominant expression and induction early in adipocyte differentiation, Endocrinology 135 (1994) 798–800.
[9] K.T. Dalen, K. Schoonjans, S.M. Ulven, M.S. Weedon-Fekjaer, T.G. Bentzen, H. Koutnikova, J. Auwerx, H.I. Nebbl, Adipose tissue expression of the lipid droplet-associating proteins S3-12 and perilipin is controlled by peroxisome proliferator-activated receptor-gamma, Diabetes 53 (2004) 1243–1252.
[10] P. Tontonoz, E. Hu, B.M. Spiegelman, Stimulation of adipogenesis in fibroblasts by PPAR gamma 2, a lipid-activated transcription factor, Cell 79 (1994) 1147–1156.
[11] W. He, Y. Barak, A. Hevener, P. Olson, D. Liao, J. Le, M. Nelson, E. Ong, J.M. Olefsky, R.M. Evans, Adipose-specific peroxisome proliferator-activated receptor gamma knockout causes insulin resistance in fat and liver but not in muscle, Proc. Natl. Acad. Sci. U. S. A. 100 (2003) 15712–15717.
[12] M.J. Barrero, N. Camarero, P.F. Marrero, D. Haro, Control of human carnitine palmitoyltransferase II gene transcription by peroxisome proliferator-activated receptor through a partially conserved peroxisome proliferator-responsive element, Biochem. J. 369 (2003) 721–729.
[13] S. Mandard, M. Muller, S. Kersten, Peroxisome proliferator-activated receptor alpha target genes, Cell. Mol. Life Sci.: CM 61 (2004) 393–416.
[14] A. Moldes-Anaya, T. Saether, S. Uhlig, H.I. Nebb, T. Larsen, H.C. Eilertsen, S.M. Paulsen, Two isomeric C16 oxo-fatty acids from the Diatom Chaetoceros karianus show dual agonist activity towards human peroxisome proliferator-activated receptors (PPARs) alpha/gamma, Mar. Drugs 15 (2017).
[15] B. Qu, Q.-T. Li, K.P. Wong, T.M.C. Tan, B. Halliwell, Mechanism of clofibrate hepatotoxicity: mitochondrial damage and oxidative stress in hepatocytes, Free Radic. Biol. Med. 31 (2001) 659–669.
[16] E.A.M. Gale, Lessons from the glitazones: a story of drug development, Lancet 357 (2001) 1870–1875.
[17] I.B. Hirsch, J. Kelly, S. Cooper, Pulmonary edema associated with troglitazone therapy, Arch. Intern. Med. 159 (1999) 1811–1817.
[18] S.E. Nissen, K. Wolski, Effect of rosiglitazone on the risk of myocardial infarction and death from cardiovascular causes, N. Engl. J. Med. 356 (2007) 2457–2471.
[19] H.E. Lebovitz, J.F. Dole, R. Patwardhan, E.B. Rappaport, M.I. Freed, Rosiglitazone monotherapy is effective in patients with type 2 diabetes, J. Clin. Endocrinol. Metabol. 86 (2001) 280–288.
[20] A.V. Schwartz, D.E. Sellmeyer, E. Vittinghoff, L. Palermo, B. Lecka-Czernik, K.R. Feingold, E.S. Strotmeyer, H.E. Resnick, L. Carbone, B.A. Beamer, S.W. Park, N.E. Lane, T.B. Harris, S.R. Cummings, Thiazolidinedione use and bone loss in older diabetic adults, J. Clin. Endocrinol. Metabol. 91 (2006) 3349–3354.
[21] M. Ferwana, B. Firwana, R. Hasan, M.H. Al-Mallah, S. Kim, V.M. Montori, M.H. Murad, Pioglitazone and risk of bladder cancer: a meta-analysis of controlled studies, Diabet. Med. 30 (2013) 1026–1032.
[22] J.D. Lewis, L.A. Habel, C.P. Quesenberry, et al., Pioglitazone use and risk of bladder cancer and other common cancers in persons with diabetes, J. Am. Med. Assoc. 314 (2015) 265–277.
[23] M.R. Jain, S.R. Giri, C. Trivedi, B. Bhoi, A. Rath, G. Vanage, P. Vyas, R. Ranvir, P.R. Patel, Saroglitazar, a novel PPARalpha/gamma agonist with predominant PPARalpha activity, shows lipid-lowering and insulin-sensitizing effects in preclinical models, Pharmacol. Res.Perspect. 3 (2015) e00136.
[24] C.K. Tan, Y. Zhuang, W. Wahli, Synthetic and natural Peroxisome Proliferator-Activated Receptor (PPAR) agonists as candidates for the therapy of the metabolic syndrome, Expert Opin. Ther. Targets 21 (2017) 333–348.
[25] A. Benardeau, P. Verry, E.A. Atzpodien, J.M. Funk, M. Meyer, J. Mizrahi, M. Winter, M.B. Wright, S. Uhles, E. Sebokova, Effects of the dual PPAR-alpha/gamma agonist aleglitazar on glycaemic control and organ protection in the Zucker diabetic fatty rat, Diabetes Obes. Metabol. 15 (2013) 164–174.
[26] F. Gilardi, M. Giudici, N. Mitro, O. Maschi, U. Guerrini, G. Rando, A. Maggi, G. Cermenati, A. Laghezza, F. Loiodice, G. Pochetti, A. Lavecchia, D. Caruso, E. De Fabiani, K. Bamberg, M. Crestani, LT175 is a novel PPARalpha/gamma ligand with potent insulin-sensitizing effects and reduced adipogenic properties, J. Biol. Chem. 289 (2014) 6908–6920.
[27] S. Kasai, T. Inoue, H. Yoshitomi, T. Hihara, F. Matsuura, H. Harada, M. Shinoda, I. Tanaka, Antidiabetic and hypolipidemic effects of a novel dual peroxisome proliferator-activated receptor (PPAR) alpha/gamma agonist, E3030, in db/db mice and beagle dogs, J. Pharmacol. Sci. 108 (2008) 40–48.
[28] M. Aursnes, J.E. Tungen, A. Vik, R. Colas, C.Y. Cheng, J. Dalli, C.N. Serhan, T.V. Hansen, Total synthesis of the lipid mediator PD1n-3 DPA: configurational assignments and anti-inflammatory and pro-resolving actions, J. Nat. Prod. 77 (2014) 910–916.
[29] K. Kai, J. Takeuchi, T. Kataoka, M. Yokoyama, N. Watanabe, Structure–activity relationship study of flowering-inducer FN against Lemna paucicostata, Tetrahedron 64 (2008) 6760–6769.
[30] M.J. Cryle, P.Y. Hayes, J.J. De Voss, Enzyme-substrate complementarity governs

access to a cationic reaction manifold in the P450(BM3)-catalysed oxidation of cyclopropyl fatty acids, Chemistry 18 (2012) 15994–15999.
[31] I. Borbath, Y. Horsmans, The role of PPARgamma in hepatocellular carcinoma, PPAR Res. 2008 (2008) 209520.
[32] M. Wabitsch, R.E. Brenner, I. Melzner, M. Braun, P. Moller, E. Heinze, K.M. Debatin, H. Hauner, Characterization of a human preadipocyte cell strain with high capacity for adipose differentiation, Int. J. Obes. Relat. Metab. Disord. 25 (2001) 8–15.
[33] L.M. DiPilato, F. Ahmad, M. Harms, P. Seale, V. Manganiello, M.J. Birnbaum, The role of PDE3B phosphorylation in the inhibition of lipolysis by insulin, Mol. Cell Biol. 35 (2015) 2752–2760.
[34] S.M. Kraynik, R.S. Miyaoka, J.A. Beavo, PDE3 and PDE4 isozyme-selective inhibitors are both required for synergistic activation of brown adipose tissue, Mol. Pharmacol. 83 (2013) 1155–1165.
[35] J. Wilding, Thiazolidinediones, insulin resistance and obesity: finding a balance, Int. J. Clin. Pract. 60 (2006) 1272–1280.
[36] W. Tang, D. Zeve, J. Seo, A.Y. Jo, J.M. Graff, Thiazolidinediones regulate adipose lineage dynamics, Cell Metabol. 14 (2011) 116–122.
[37] P. Hallenborg, R.K. Petersen, I. Kouskoumvekaki, J.W. Newman, L. Madsen, K. Kristiansen, The elusive endogenous adipogenic PPARgamma agonists: lining up the suspects, Prog. Lipid Res. 61 (2016) 149–162.
[38] I. Tzameli, H. Fang, M. Ollero, H. Shi, J.K. Hamm, P. Kievit, A.N. Hollenberg, J.S. Flier, Regulated production of a peroxisome proliferator-activated receptor-gamma ligand during an early phase of adipocyte differentiation in 3T3-L1 adipocytes, J. Biol. Chem. 279 (2004) 36093–36102.
[39] J.B. Kim, H.M. Wright, M. Wright, B.M. Spiegelman, ADD1/SREBP1 activates PPARgamma through the production of endogenous ligand, Proc. Natl. Acad. Sci. U. S. A. 95 (1998) 4333–4337.
[40] T. Itoh, L. Fairall, K. Amin, Y. Inaba, A. Szanto, B.L. Balint, L. Nagy, K. Yamamoto, J.W. Schwabe, Structural basis for the activation of PPARgamma by oxidized fatty acids, Nat. Struct. Mol. Biol. 15 (2008) 924–931.
[41] T. Shiraki, N. Kamiya, S. Shiki, T.S. Kodama, A. Kakizuka, H. Jingami, Alpha,-beta-unsaturated ketone is a core moiety of natural ligands for covalent binding to peroxisome proliferator-activated receptor gamma, J. Biol. Chem. 280 (2005) 14145–14153.
[42] Å. Kaupang, T. Laitinen, A. Poso, T.V. Hansen, Structural review of PPARγ in complex with ligands: cartesian- and dihedral angle principal component analyses of X-ray crystallographic data, Protein.Struct.Funct.Bioinformatics 85 (2017) 1684–1698.
[43] L. Piemontese, G. Fracchiolla, A. Carrieri, M. Parente, A. Laghezza, G. Carbonara, S. Sblano, M. Tauro, F. Gilardi, P. Tortorella, A. Lavecchia, M. Crestani, B. Desvergne, F. Loiodice, Design, synthesis and biological evaluation of a class of bioisosteric oximes of the novel dual peroxisome proliferator-activated receptor alpha/gamma ligand LT175, Eur. J. Med. Chem. 90 (2015) 583–594.
[44] R. Cancello, C. Henegar, N. Viguerie, S. Taleb, C. Poitou, C. Rouault, M. Coupaye, V. Pelloux, D. Hugol, J.L. Bouillot, A. Bouloumie, G. Barbatelli, S. Cinti, P.A. Svensson, G.S. Barsh, J.D. Zucker, A. Basdevant, D. Langin, K. Clement, Reduction of macrophage infiltration and chemoattractant gene expression changes in white adipose tissue of morbidly obese subjects after surgery-induced weight loss, Diabetes 54 (2005) 2277–2286.
[45] Y.E. Kang, J.M. Kim, K.H. Joung, J.H. Lee, B.R. You, M.J. Choi, M.J. Ryu, Y.B. Ko, M.A. Lee, J. Lee, B.J. Ku, M. Shong, K.H. Lee, H.J. Kim, The roles of adipokines, proinflammatory cytokines, and adipose tissue macrophages in obesity-associated insulin resistance in modest obesity and early metabolic dysfunction, PLoS One 11 (2016) e0154003.
[46] D. Gao, M. Madi, C. Ding, M. Fok, T. Steele, C. Ford, L. Hunter, C. Bing, Interleukin-1beta mediates macrophage-induced impairment of insulin signaling in human primary adipocytes, American journal of physiology, Endocrinol. Metabol. 307 (2014) E289–E304.
[47] D. Gao, P. Trayhurn, C. Bing, 1,25-Dihydroxyvitamin D3 inhibits the cytokine-induced secretion of MCP-1 and reduces monocyte recruitment by human preadipocytes, Int. J. Obes. 37 (2013) 357–365.
[48] C. Bing, Is interleukin-1beta a culprit in macrophage-adipocyte crosstalk in obesity? Adipocyte 4 (2015) 149–152.
[49] S. Sugii, P. Olson, D.D. Sears, M. Saberi, A.R. Atkins, G.D. Barish, S.H. Hong, G.L. Castro, Y.Q. Yin, M.C. Nelson, G. Hsiao, D.R. Greaves, M. Downes, R.T. Yu, J.M. Olefsky, R.M. Evans, PPARgamma activation in adipocytes is sufficient for systemic insulin sensitization, Proc. Natl. Acad. Sci. U. S. A. 106 (2009) 22504–22509.
[50] P. Mohanty, A. Aljada, H. Ghanim, D. Hofmeyer, D. Tripathy, T. Syed, W. Al-Haddad, S. Dhindsa, P. Dandona, Evidence for a potent antiinflammatory effect of rosiglitazone, J. Clin. Endocrinol. Metab. 89 (2004) 2728–2735.
[51] C. Lagathu, L. Yvan-Charvet, J.P. Bastard, M. Maachi, A. Quignard-Boulange, J. Capeau, M. Caron, Long-term treatment with interleukin-1beta induces insulin resistance in murine and human adipocytes, Diabetologia 49 (2006) 2162–2173.
[52] J. Jager, T. Gremeaux, M. Cormont, Y. Le Marchand-Brustel, J.F. Tanti, Interleukin-1beta-induced insulin resistance in adipocytes through down-regulation of insulin receptor substrate-1 expression, Endocrinology 148 (2007) 241–251.
[53] D. Lucet, P. Heyse, A. Gissot, T.L. Gall, C. Mioskowski, Synthesis of the diastereomers of dethiobiotin using the conjugate addition of 4-Phenyloxazolidin-2-one to a nitroalkene, Eur. J. Org Chem. 2000 (2000) 3575–3579.
[54] J.T. Starr, G. Koch, E.M. Carreira, Enantioselective synthesis of the cyclopentyl core of the axinellamines, J. Am. Chem. Soc. 122 (2000) 8793–8794.
[55] M.S. Weedon-Fekjaer, K.T. Dalen, K. Solaas, A.C. Staff, A.K. Duttaroy, H.I. Nebb, Activation of LXR increases acyl-CoA synthetase activity through direct regulation of ACSL3 in human placental trophoblast cells, J. Lipid Res. 51 (2010) 1886–1896.
[56] L. Napal, P.F. Marrero, D. Haro, An intronic peroxisome proliferator-activated receptor-binding sequence mediates fatty acid induction of the human carnitine palmitoyltransferase 1A, J. Mol. Biol. 354 (2005) 751–759.
[57] J. Ye, G. Coulouris, I. Zaretskaya, I. Cutcutache, S. Rozen, T.L. Madden, Primer-BLAST: a tool to design target-specific primers for polymerase chain reaction, BMC Bioinf. 13 (2012) 134.
[58] T. Metsalu, J. Vilo, ClustVis: a web tool for visualizing clustering of multivariate data using principal component analysis and heatmap, Nucleic Acids Res. 43 (2015) W566–W570.
[59] R. Herwig, C. Hardt, M. Lienhard, A. Kamburov, Analyzing and interpreting genome data at the network level with ConsensusPathDB, Nat. Protoc. 11 (2016) 1889–1907.